DESIGN OF A GRID FIN AERODYNAMIC CONTROL DEVICE FOR TRANSONIC FLIGHT REGIME

A THESIS SUBMITTED TO
THE GRADUATE SCHOOL OF NATURAL AND APPLIED SCIENCES
OF
MIDDLE EAST TECHNICAL UNIVERSITY

BY

ERDEM DİKBAŞ

IN PARTIAL FULFILLMENT OF THE REQUIREMENTS
FOR
THE DEGREE OF MASTER OF SCIENCE
IN
MECHANICAL ENGINEERING

JUNE 2015

Approval of the thesis:

DESIGN OF A GRID FIN AERODYNAMIC CONTROL DEVICE FOR TRANSONIC FLIGHT REGIME

submitted by **ERDEM DİKBAŞ** in partial fulfillment of the requirements for the degree of **Master of Science in Mechanical Engineering Department, Middle East Technical University** by,

Prof. Dr. Gülbin Dural Ünver
Dean, Graduate School of **Natural and Applied Sciences** _____

Prof. Dr. Tuna Balkan
Head of Department, **Mechanical Engineering** _____

Assist. Prof. Dr. Cüneyt Sert
Supervisor, **Mechanical Engineering Dept., METU** _____

Assist. Prof. Dr. Özgür Uğraş Baran
Co-supervisor, **Mechanical Engineering Dept., TED Uni.** _____

Examining Committee Members:

Prof. Dr. M. Haluk Aksel
Mechanical Engineering Department, METU _____

Assist. Prof. Dr. Cüneyt Sert
Mechanical Engineering Department, METU _____

Assist. Prof. Dr. Özgür Uğraş Baran
Mechanical Engineering Department, TED Uni. _____

Assoc. Prof. Dr. M. Metin Yavuz
Mechanical Engineering Department, METU _____

Assist. Prof. Dr. Nilay Sezer Uzol
Mechanical Engineering Department, TOBB ETÜ _____

Date: June 3, 2015

I hereby declare that all information in this document has been obtained and presented in accordance with academic rules and ethical conduct. I also declare that, as required by these rules and conduct, I have fully cited and referenced all material and results that are not original to this work.

Name, Last Name: ERDEM DİKBAŞ

Signature :

ABSTRACT

DESIGN OF A GRID FIN AERODYNAMIC CONTROL DEVICE FOR TRANSONIC FLIGHT REGIME

Dikbaş, Erdem
M.S., Department of Mechanical Engineering
Supervisor : Assist. Prof. Dr. Cüneyt Sert
Co-Supervisor : Assist. Prof. Dr. Özgür Uğraş Baran

June 2015, 84 pages

Grid fins is unconventional control devices and they are used for aerodynamic control of various types of missiles. Low hinge moment requirement and superior packaging possibilities make grid fins attractive when compared to conventional planar fins. However, design of grid fins is more involved when transonic flight regime is considered. The reason for this is high drag force encountered by the grid fin. The purpose of the thesis is to overcome this drawback and to define a proper design methodology for transonic flight regime. Computational Fluid Dynamics (CFD) is utilized as main tool in calculation of aerodynamic force and moments. Computational efforts are significantly easified by utilization of 'unit grid fin' concept, which is introduced in this thesis study. At the end, an equivalent control performance is accomplished with a more efficient design when compared to a conventional planar fin example.

Keywords: Grid Fin, Lattice Fin, Missile Aerodynamic Control, Transonic Flow, Computational Fluid Dynamics

ÖZ

TRANSONİK HIZLARDA IZGARA TİPİ KONTROL KANATÇIĞI TASARIMI

Dikbaş, Erdem
Yüksek Lisans, Makina Mühendisliği Bölümü
Tez Yöneticisi : Yrd. Doç. Dr. Cüneyt Sert
Ortak Tez Yöneticisi : Yrd. Doç. Dr. Özgür Uğraş Baran

Haziran 2015 , 84 sayfa

Izgara tipi kanatçıklar, değişik türde mühimmatların aerodinamik kontrolünü sağlayan, alışılmadık kontrol kanatçıklarındandır. Yarattığı düşük menteşe momenti ve kolay katlanabilmesi, ızgara tipi kanatçıkları, alışıldık düzlemsel kanatçıklara göre tercih edilebilir kılmaktadır. Fakat, ızgara tipi kanatçıkların tasarımı, transonik uçuş koşulları düşünüldüğünde, çok daha zordur. Bunun sebebi, ızgara tipi kanatçıkların, bu koşullarda daha fazla sürükleme kuvveti oluşturmasıdır. Tezin amacı, bu zorluğun üstesinden gelebilmek ve transonik uçuş şartları için uygun bir tasarım metodolojisi tanımlayabilmektir. Bu tezde, aerodinamik kuvvet ve momentleri hesaplanmasında, Hesaplamalı Akışkanlar Dinamiği (HAD) temel araç olarak kullanılmıştır. Hesaplama gereksinimleri, bu tezde tanıtılmış olan 'birim kanatçık' kavramının kullanımıyla önemli miktarda azaltılmıştır. Tezin sonunda, bir konvansiyonel düzlemsel kanatçıkla eşdeğer bir kontrol performansı sergileyen ve aynı zamanda ondan daha verimli çalışan bir

ızgara tipi kanatçık tasarlanmıştır.

Anahtar Kelimeler: Izgara Tipi Kanatçık, Füze Aerodinamik Kontrolü, Transonik Akış, Hesaplamalı Akışkanlar Dinamiği

To My Grandfather

ACKNOWLEDGMENTS

I wish my deepest gratitude to my supervisor, Assist. Prof. Dr. Cüneyt Sert, for his guidance, advice and criticism throughout the thesis.

I am also grateful to my co-supervisor, Assist. Prof. Dr. Özgür Uğraş Baran, for his endless support, supervision and encouragements. Without him this thesis would not be completed.

I am thankful to my girlfriend, Tuğçe Topaloğlu, for her mental support. Her love has always been a source of motivation for this thesis study.

I would like to thank my colleagues in Flight Mechanics Division of TÜBİTAK-SAGE, where the efforts on the thesis study were being carried out. Experiences that I gained there were also helpful in this study. I also want to express my gratitude to Head of Flight Mechanics Division, Dr. Ümit Kutluay, for the convenience provided by him.

A part of the numerical calculations reported in this thesis were performed at TÜBİTAK-ULAKBİM, High Performance and Grid Computing Center (TRUBA Resources).

I finally would like to thank anyone who has supported my thesis effort in any way.

TABLE OF CONTENTS

LIST OF TABLES

TABLES

LIST OF FIGURES

FIGURES

LIST OF SYMBOLS

Symbols

$\hat{i}$	Unit vector in x-direction of body/UGF coordinate system
$\hat{j}$	Unit vector in y-direction of body/UGF coordinate system
$\hat{k}$	Unit vector in z-direction of body/UGF coordinate system
CA	Axial force coefficient
CN	Normal force coefficient
CL	Lift coefficient
CD	Drag coefficient
α	Angle of attack
α_{eff}	Effective/local angle of attack
CN_{α}	Normal force slope
Cm_{α}	Stability parameter
$Cm_{\delta e}$	Pitch control parameter
Cm_h	Hinge moment
$\frac{\alpha}{\delta e}$	Pitch control effectiveness
δa	Aileron deflection
δe	Elevator deflection
δr	Rudder deflection
M	Mach number
$\vec{V}$	Velocity vector
W	Weight of an aircraft
s	Span
b	Total width
c	Chord length
w	Width
t	Thickness
t_f	Frame thickness
θ	Leading edge sharpness angle

ω	Backsweep angle
γ	Specific heat ratio
μ	Mach cone angle
ρ	Density
p	Pressure
S_{ref}	Reference area
l_{ref}	Reference length
n	Number of repetitions of UGF in a grid fin
D	Diameter of missile body

Subscripts

$trim$	Trimmed properties
∞	Freestream properties
cr	Critical properties
u	Upstream properties
e	Exit properties
M	Missile-body-only properties
GF	Grid-fin-only properties
MGF	Missile with grid fin properties
BF	Basic Finner properties

CHAPTER 1

INTRODUCTION

Grid fins, alternatively called lattice fins, lattice wings, *etc.*, are unconventional missile control surfaces used in place of regular planar fins. They make use of internal framework of planar surfaces arranged to generate required aerodynamic force which creates a moment at the center of gravity of missile.

Grid fins have been used in aerospace vehicles since 1970s. Various Soviet ballistic missiles and Soyuz spacecraft were equipped with grid fins; however, their use did not cover control purposes. They served mostly as air brake systems and stabilization units. There are a few applications of supersonic missiles, most of which are also Russian made. One of the most famous examples of these is beyond visual range air-to-air missile 'Vympel R-77' (see Fig. 1.1), which has a control unit operating with grid fin devices. American made large-scale guided bomb 'Massive Ordnance Air Blast' contains a set of four grid fins as seen in Fig. 1.2. As a very recent notice (November 2014), Falcon 9 launch vehicle of SpaceX company makes use of grid fins in order to achieve an enhanced precision landing onto an off-shore barge [1].

1.1 Aerodynamic Control of Missiles

Control and maneuvering of missiles are done in two ways, which are usually referred to as conventional and unconventional flight control alternatives. Unconventional flight control covers thrust vector control (TVC) and jet interaction control [3], while conventional aerodynamic control is applied through deflection

Figure 1.1: Vympel R-77 with grid fins [2]

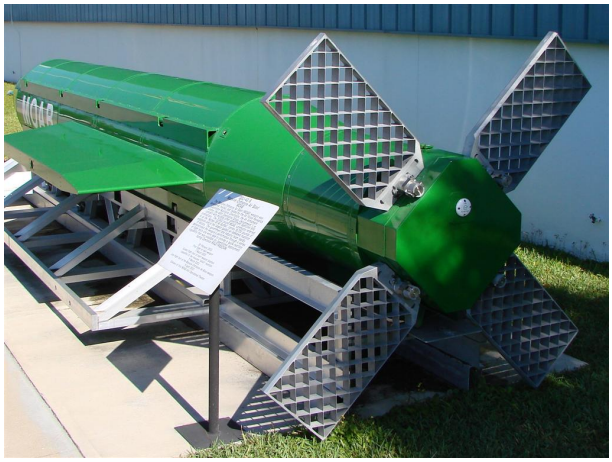

Figure 1.2: MOAB with grid fins [2]

of lifting surfaces. Conventional aerodynamic control is classified with regard to placement of control surfaces. Fig. 1.3 shows these three common alternatives.

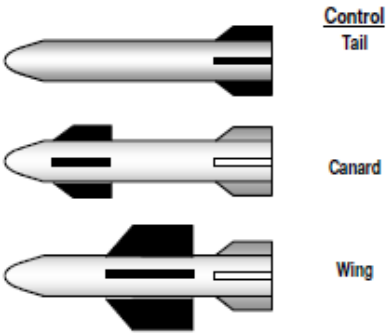

Figure 1.3: Aerodynamic control alternatives [3]

In tail control, it is a common practice that control surfaces are designed as tail fins themselves. In other words, tail stabilizer fins act as control elements, in addition to their primary purpose, which is to provide a stable flight for an air vehicle. To accomplish this, each tail fin has the ability to rotate about a certain axis along which an excitation device, such as a hydraulic and an electric motor, is in action. Tail control aims to create sufficient amount of moment at the center of gravity of the missile in order to generate desired lift force.

Wing control is achieved by deflecting the whole wing so that it creates a lift force to maneuver the missile. As it does not require body rotation to generate lift force, wing control usually responses faster than tail and canard controls. However, displacement of a large wing necessitates strong actuators [3].

Canard control is applied by small wings located on the forebody. Such kind of missiles also carry stabilizer fins on the aftbody. Rotating canards create sufficient moments at the center of gravity of missile, similar to tail control.

In this thesis, tail control is applied as the preferred alternative since it is the most common missile control technique. Air vehicle control is applied by three primary control deflection sets which serve at each principal axis. Aileron deflection, δa, creates rolling moment, which is the moment component in x-direction of body coordinate system. Elevator deflection, δe, creates pitching moment

in y-direction and rudder deflection, δr, leads to yawing rotation in z-direction. Principal rotation directions are given in Fig. 1.4. Pure deflection arrangements, where leading edges of fins move in the indicated directions or the opposite, are given in Fig. 1.5.

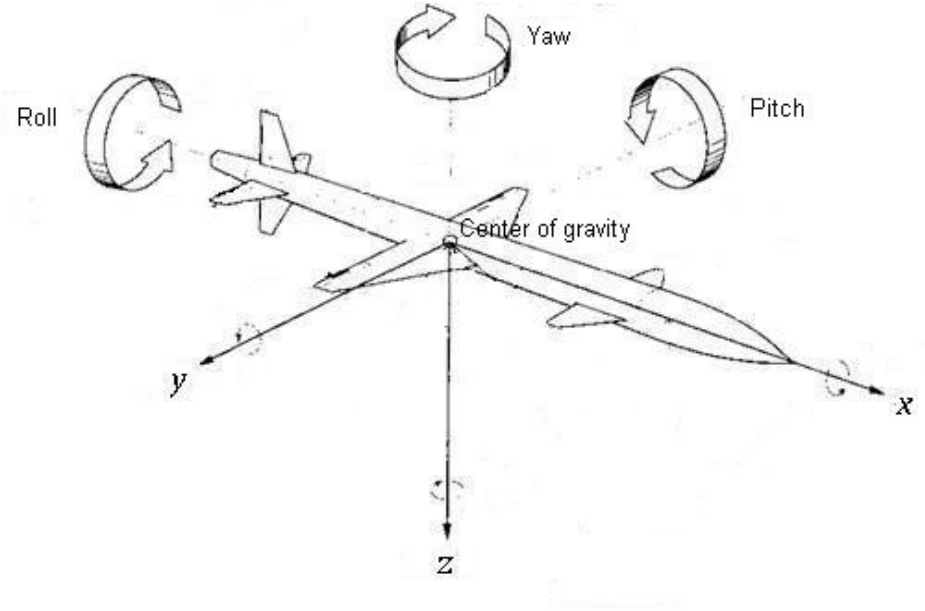

Figure 1.4: Missile body fixed coordinate system and principal rotations [4]

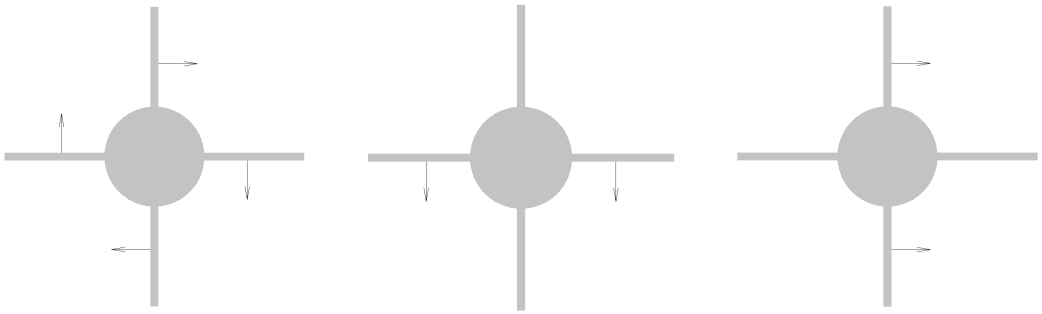

(a) Aileron (b) Elevator (c) Rudder

Figure 1.5: Pure deflection arrangements of control fins

Pitching moment is created by the technique shown in Fig. 1.6. Negative deflection creates a positive moment at the center of gravity. In order to sustain a flight in equilibrium, which is usually referred to as trimmed flight, two conditions must be satisfied:

1. Lift force on whole missile must be equal to weight.

2. Pitching moment on the whole missile must vanish.

These conditions yields a set of two algebraic equations, which are to be solved together, where α stands for angle of attack, as shown in Fig. 1.6:

1. $L = f_1(\alpha, \delta e) = W$

2. $m = f_2(\alpha, \delta e) = 0$

Solution of the set of equations results in a unique couple of $[\alpha_{trim}, \delta e_{trim}]$. This means that, at a certain flight condition (i.e. fixed Mach number and altitude), an equilibrium flight in pitch axis is achieved by deflecting the fins in elevator direction. Yaw control is performed in a similar method, either.

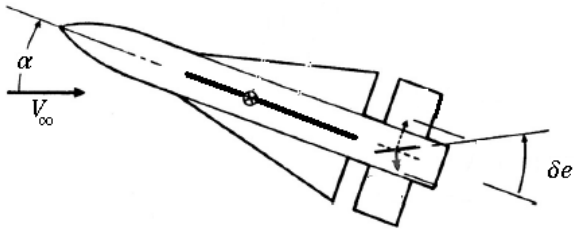

Figure 1.6: Generating pitching moment in trimmed flight [3]

Pitch control is taken as the only concern in this thesis. It represents also the characteristics of yaw control when geometry of the air vehicle is symmetric with respect to diagonal plane (see $y = z$ plane in Fig. 1.4). Roll control is treated as less significant because critical maneuvers are handled by pitch and yaw controls in most of the mission profiles.

1.2 Grid Fin in General

Grid fins are aerodynamic control devices operated by the same principle that is explained in Section 1.1. Unlike the planar fin, air flow passes through the

grid fin lattices and generates the aerodynamic force by interacting with internal surface pattern.

Guidance with grid fin is achieved by deflecting the fins from their original positions. Doing this, relative air flow changes its direction and aerodynamic lift force is generated. A grid fin rotates about its rotation axis, which is referred to as "hinge line", with the aid of an actuator motor aligned with the fin centerline. Fin centerline is defined as the axis passing through geometric center of fin and parallel to yz-plane of the missile (see Fig. 1.4 for yz-plane). As a result, guidance commands coming into fin actuators create a rotational motion about the hinge line of each grid fin, as shown in Fig. 1.7.

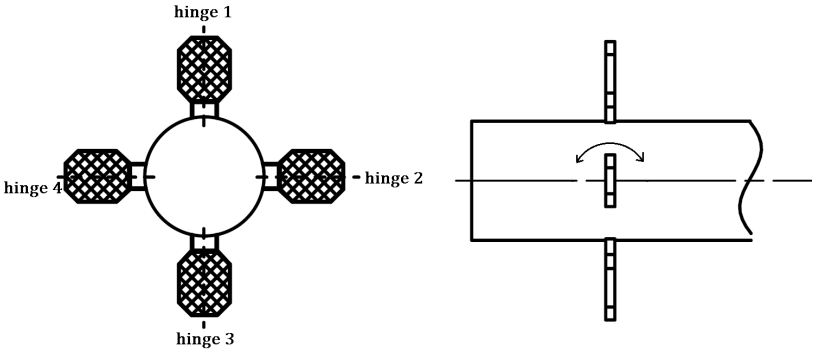

Figure 1.7: Hinge lines of generic cruciform set of grid fins

Use of grid fins provides both advantages and disadvantages in a few aspects. First of all, a missile with grid fin can achieve a stronger maneuverability in low subsonic and high supersonic flight conditions. However, transonic and low supersonic speeds are considered as problematic due to low effectiveness and high drag characteristics. Therefore, to control a missile operated in transonic flight, the grid fins should be carefully designed. The second advantage is introduced as low hinge moment requirement, which reduces the costs of actuator motor and gearbox equipments. As a disadvantage, grid fins yield a high radar cross section (RCS) as a result of high number of surfaces. Also, high transonic drag can be included in the disadvantages.

A distinctive feature of grid fin is introduced as superior packaging capability,

which those missiles displaced from an internal weapon bay or from a launcher tube (see Fig. 1.8b) necessitate. Geometric design of such kind of missiles is mainly driven by the enclosing volume of the launcher station. For this reason, while they are kept in this limited volume before launch, it is most probably necessary to stow fins on the body of missile. This mechanism is applied easily when grid fins are utilized, as seen in Fig. 1.8a.

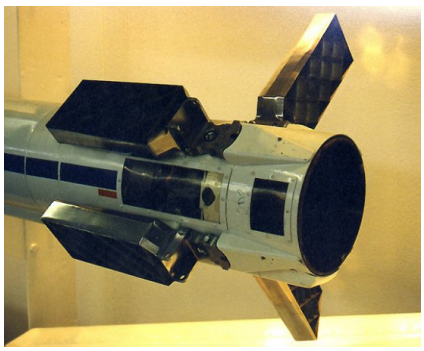

(a) Stowed grid fins on Vympel R-77 [5]

(b) A tube launcher (BGM-71) [6]

Figure 1.8: Easy packaging of grid fins

1.3 Existing Literature

Research and development studies on grid fin are first conducted by Belotserkovsky (or Belocerkovsky, Belotzerkovskii) *et al.* and their work is gathered in the book "Lattice Wings" in 1985 [7]. In this book, basic assessments for grid fins are examined in aerodynamics, structural mechanics and manufacturing technologies disciplines. In aerodynamic point of view, flow field characteristics under different flight regimes have been explained. Aerodynamic force prediction methods, such as vortex lattice method and linear theory, have been utilized and applied for grid fin flow field in appropriate flight conditions.

The flow field around lattice surfaces of a grid fin is classified by flight regimes which are distinguished with well-defined Mach number thresholds. Three critical Mach number values, which are comprehensively discussed in Section 2.3, define the flight condition intervals, in which distinctive flow characteristics are observed, as exemplified in Fig. 1.9. Transonic flight of a missile with grid

fins primarily suffers from high drag force. The reason for elevated drag is the internal flow field characteristics within the cube-like cells of grid fins. In the transonic regime, the flow inside the cells is choked and flow in upstream of the fins decelerates. This means that grid fins act as an obstacle to the flow so that drag force increases [8].

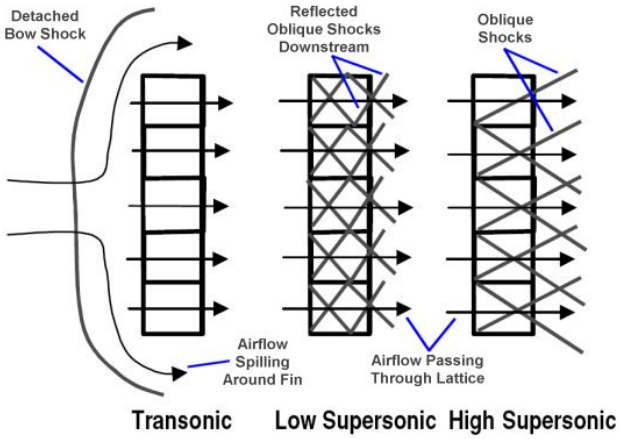

Figure 1.9: Flow patterns in different flight conditions [5]

Prediction of lift and drag forces on a grid fin has always been a popular topic since the early research studies were conducted. Theoretical and experimental studies have concentrated on behavior of grid fin on a missile body. Burkhalter *et al.*, who are one of the users of vortex lattice method for grid fin configurations, developed a theoretical calculation method for subsonic operation of grid fin isolated from body [9] and they defined an upwash effect of body which has to be taken into account at non-zero angles of attack [10]. Later, Theertamalai applied body upwash theory to this method and obtained satisfactory results [11]. The study, afterwards, was extended to a wide range of Mach numbers by the same researchers and it is shown that the theoretical methods are accurate only for small effective angles of attack on grid fins [12].

It is understandable that comparison of grid fins with conventional planar fins is one of the issues of interest. Existing literature has pointed out the differences between these two control concepts in a wide range of flight conditions. Primary advantage of using grid fins comes with significantly low magnitudes of hinge moment and minimal variation of center of pressure with changing flight

conditions [13]. On the other hand, grid fin is likely to be subject to high axial force for large number of lattice surfaces; however, it is possible to deal with this by careful web and frame design [14]. It is also reported that a weaker control effectiveness is achieved in transonic range of speeds with the use of grid fins when comparable static stability is assured for missile with the use of both types of fins [13]. Moreover, analysis of planar and grid fins that are of similar dimensions showed that the latter has superior hinge moment performance, yet the only disadvantage is seen as drag characteristics for all ranges of Mach numbers [15].

Experimental analyses on grid fins provide an invaluable source for validation of theoretical and computational prediction methods. Washington and Miller [14] conducted numerous experiments that covered different flight regimes as well as geometric parameters. Their results on aerodynamic force and hinge moment values were frequently referred in subsequent studies [16–18].

Operation performance of grid fin is highly dependent on the flight conditions, i.e., Mach number of flow. It is known that lift curve slope, which indicates the effectiveness of a control fin, diminishes in transonic speeds due to formation of shock waves inside the grid fin cells. For transonic Mach numbers below unity, Belotserkovsky *et al.* formulated this decrease as magnitude of loss of dynamic pressure due to choking that occurs within the cells [7]. This fact was also shown experimentally by Abate and Duckerschein [19]. A more systematic approach, relating the geometric parameters with choking phenomenon, was held during the wind tunnel tests conducted at Aeroballistic Research Facility to show the discontinuity of control effectiveness nearby the critical Mach number [20]. Normal force and pitch moment coefficient data obtained from these tests clearly indicate the loss in the control effectiveness, which is usually referred to as 'transonic bucket' in literature (see Fig. 1.10).

CFD analyses of grid fins took part in the literature relatively late owing to developing computer technology after 2000. As the solutions of problems including grid fins require a denser computational mesh for their lattice geometry, it is more difficult to obtain accurate results when compared to solutions with

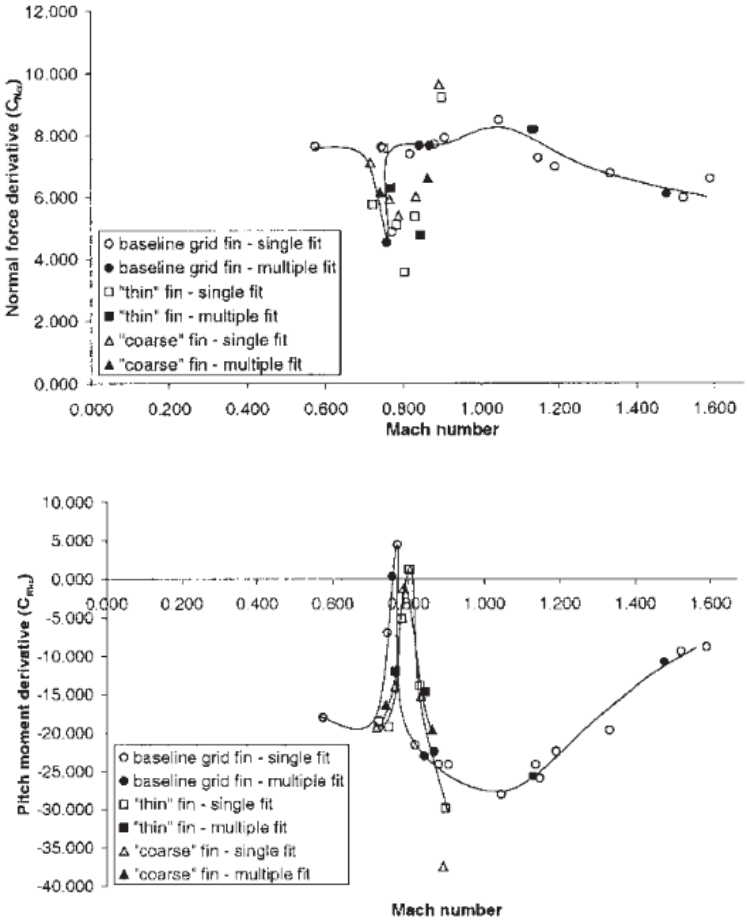

Figure 1.10: Transonic bucket shown by Abate *et al.* [20]

conventional planar fins. Nevertheless, agreement with experimental results has been accomplished for subsonic, transonic [18, 21] and supersonic [22] range of speeds.

Although most CFD analyses have been carried out by viscous models, there exists an inviscid investigation with the use of Cartesian grid [23]. In this study, a set of grid fins is mounted on a launch abort vehicle (LAV) and computations are carried out in subsonic, transonic and supersonic speed ranges. The comparison with experimental results has shown that Euler solutions were quite acceptable for supersonic Mach numbers.

Upwash and downwash effects on a grid fin, which occur due to flow field created by missile body, were studied in Theerthamalai and Nagarathinam's supersonic

analysis [24]. This study shows that the orientation of grid fin set (+ or $\times$ configuration) is important in terms of aerodynamic loads.

Efforts on reducing the transonic drag penalty are becoming popular and this issue is currently being the main concern related to grid fin applications. Drag force on a grid fin at transonic speeds increases due to choking for Mach numbers below unity and shock reflections for those larger than unity. These occurrences were qualitatively examined and their conditions were explained in detail [25]. Sharp leading edge and sweptback models (see Fig. 1.11) are examples to solutions to remedy the excessive drag problem. Significant decrease were achieved with use of those models [26,27]. Moreover, their minimal effect on lifting performance had already been shown by Washington *et al.* [28]. Although sweptback model is convex to flow, a concave model can be developed to account the geometric compatibility with a generic missile body. It was shown that the concave curved grid fin model worked well in terms of transonic and supersonic drag reduction [29]. Furthermore, locally swept grid fins shown in Fig. 1.12, where sweeping is done for each individual cell, were validated as an effective tool for supersonic drag reduction, employing the sharp corners that diminish the strength of shock waves [30].

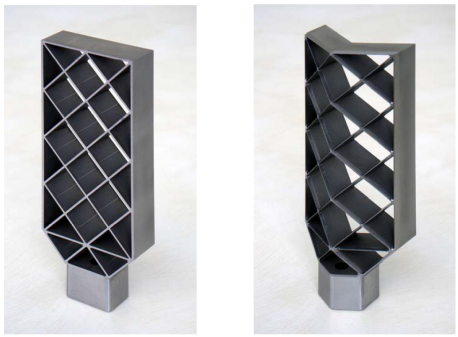

Figure 1.11: Flat (left) and sweptback (right) grid fin models [26]

1.4 Current Study

In this thesis study, application of grid fin control devices in transonic flight regime is investigated. The motivation of the study arises from the necessity of

Figure 1.12: Flat (left), valley-type (center) and peak-type (right) grid fin models [30]

employing grid fins for controlling a transonic missile for their compactness in the case of stowing on a body. Stowing the fins is a requirement when limited space is available in the storage station before the launch.

Although there are a lot of research studies focused on understanding the aerodynamic behavior of grid fins in various flight conditions, as mentioned in Section 1.3, it is observed that there is a lack of knowledge about parametric design of grid fins. This study aims to contribute to the existing literature by presenting a design methodology for grid fins in transonic flight conditions.

The thesis study constitutes five chapters. In the next chapter, geometric parameters and flow properties of grid fins are discussed. Behavior of grid fins in different flight regimes are also explained. The third chapter covers the description and validation of the computational method used in this thesis. Aim of the design and primary assessments associated with the design methodology take part in that chapter. The methodology presented in Chapter 3 is utilized in a sample case so as to obtain results in Chapter 4. This design effort results in a grid fin model performing equivalently as a generic planar fin. This chapter covers also a further improvement in drag and packaging characteristics of the newly designed geometry. Conclusions and future work plans take part in the last chapter of the thesis.

CHAPTER 2

PROPERTIES OF GRID FINS

2.1 Geometric parameters

In this section, geometric parameters, i.e., descriptive dimensions of grid fins are introduced. Shown in Fig. 2.1 are all the geometric parameters that results in a well-defined grid fin that has flat planform and blunt leading and trailing edges. Those parameters related to overall dimensions of grid fin are called as span, s, total width, b, and chord, c. The space occupied by the grid fin is driven by these three parameters. Width, w, and thickness, t, are those describing the dimensions of the individual cells. It should be noted that 'width' is the distance measured between centerlines of the walls. In addition, frame thickness, t_f, defines the dimension of the outer frame, which is utilized as the structural element to keep the grid fin cells together.

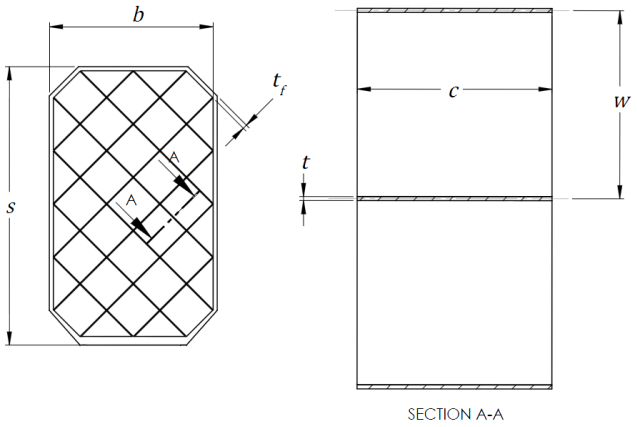

Figure 2.1: Grid fin geometric parameters

Throughout the thesis, some of the parameters introduced above are nondimensionalized, as needed. For this purpose, thickness-over-width ratio, t/w, and width-over-chord ratio, w/c, are defined in order to make interpretations of some physical phenomena, details of which is explained in detail in Section 2.2.

In addition to primary parameters introduced above, secondary parameters are defined as leading edge sharpness, θ, and backsweep angle, ω (see Fig. 2.2). Both features are invented in purpose of drag reduction in transonic flight. Leading edge sharpness provides a smoother flow, as well as it facilitates formation of oblique waves, which are more preferable than bow shock in transonic range of speed. Fig. 2.2b represents top view of a grid fin, which is swept back along its centerline, as mentioned in Section 1.3. Negative values of this parameter are also seen in the literature and these result in 'forward swept' grid fin [26].

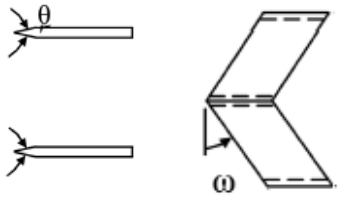

Figure 2.2: Leading edge sharpness and backsweep angle parameters [27]

2.2 Subsonic, Transonic, and Supersonic Behavior

Use of grid fin in different flight regimes results in distinctive flow characteristics which usually determine the constraints of the design efforts. In general, Subsonic ($M < 0.7$) and high supersonic ($M > 2.0$) regimes are admitted as the best performance conditions for grid fins. Even though this is a correct statement at first glance, conducting a design procedure appropriate to other Mach number ranges may result in a superior performance, too.

2.2.1 Grid Fin in Subsonic Flight

Gathered knowledge from the literature indicates that subsonic operation of grid fins is never seen as problematic because of absence of complex flow particular to this regime. Aerodynamic behavior of the grid fins is predictable with no special attention to flow field characteristics, similar to planar fins.

2.2.2 Grid Fin in Transonic Flight

Choked flow inside the grid fin cells is modeled by utilizing one-dimensional isentropic compressible flow equations in the past studies [12, 20, 25, 31, 32]. In order to be able to employ these relations, grid fin cells are considered as converging nozzles, which accelerate the upstream flow due to decreasing flow area ($A_{2-2} < A_{1-1}$, see Fig. 2.3). Depending on the area ratio ($\frac{A_{1-1}}{A_{2-2}}$) and freestream Mach number, it is possible to observe choking, when local Mach number at any region within the grid fin cell reaches to unity. For a specific Mach number, choking is observed below a certain 'critical area ratio'. This threshold can be calculated by Eq. 2.1 for any freestream Mach number [33],

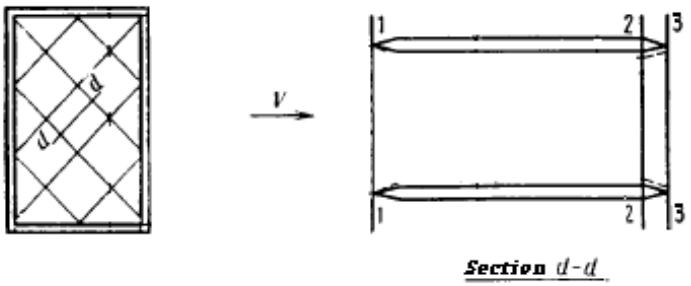

Figure 2.3: Section view of a grid fin cell [7]

$$\left(\frac{A}{A^*}\right)^2 = \frac{1}{{M_\infty}^2}\left[\frac{2}{\gamma+1}\left(1+\frac{\gamma-1}{2}{M_\infty}^2\right)\right]^{\frac{\gamma+1}{\gamma-1}} \tag{2.1}$$

where γ is the thermodynamic property of a compressible fluid and it is expressed as the ratio of specific heat capacities at constant pressure and at constant specific volume:

$$\gamma = \frac{c_p}{c_v} \tag{2.2}$$

In this equation, A^* stands for throat area, which is, by definition, the area where the flow Mach number reaches to unity. Therefore, in order to determine choking condition, A^* can be replaced with A_{2-2} and freestream flow area, i.e., A is replaced with A_{1-1}. Remembering the specific heat ratio, $\gamma = 1.4$ for air,

$$\left(\frac{A_{1-1}}{A_{2-2}}\right)_{cr} = \frac{1}{M_\infty}\left[\frac{5}{6}\left(1 + 0.2{M_\infty}^2\right)\right]^3 \tag{2.3}$$

As a result of this relation, critical area ratio is plotted as a function of freestream Mach number in Fig. 2.4.

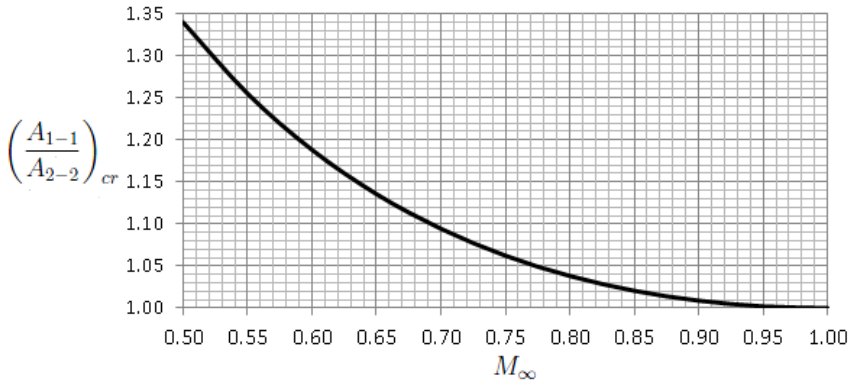

Figure 2.4: Critical area ratio vs. freestream Mach number

2.2.2.1 CFD Investigation of Choking in Grid Fin Cells

In this section, validity of converging nozzle approach for grid fins in transonic flight conditions is investigated by a computational study. For this purpose, choking in grid fin cells is observed in a two-dimensional inviscid CFD analysis within the scope of this thesis [32]. In this study, walls of grid fin is modeled as parallel plates, similar to section view in Fig. 2.3. A transonic freestream Mach number, $M_\infty = 0.80$, is selected to determine corresponding 'critical' geometry, which is expected to yield choking. At this point, critical area ratio relation (Fig. 2.3) is required to be expressed in terms of geometric parameters. Following can be written for a two-dimensional domain:

$$\left(\frac{A_{1-1}}{A_{2-2}}\right)_{cr} = \frac{w}{w - t} \tag{2.4}$$

Therefore, the relation between geometric parameters w and t, which are defined in Section 2.1, is obtained using Eq. 2.3 as:

$$\frac{w}{w-t} = \frac{1}{0.80}\left[\frac{5}{6}\left(1+0.2(0.80)^2\right)\right]^3 \tag{2.5}$$

and, it is found as, $\frac{w}{w-t} = 1.0382$. This can also be expressed as, $\frac{t}{w} = 0.0368$.

Using this geometric specification, a computational domain is created. Study is conducted in two dimensions in order to obtain the results rapidly. The schematic of the 2-D domain and the unstructured grid used in the computations is shown in Fig. 2.5. As seen in the figure, upper and lower boundaries are assigned as translational periodic to maintain periodicity during the iterations. Inflow and outflow boundary conditions are implemented through pressure-far-field boundaries, at which it is possible to assign thermodynamic parameters and an initial value for Mach number of the air flow [34].

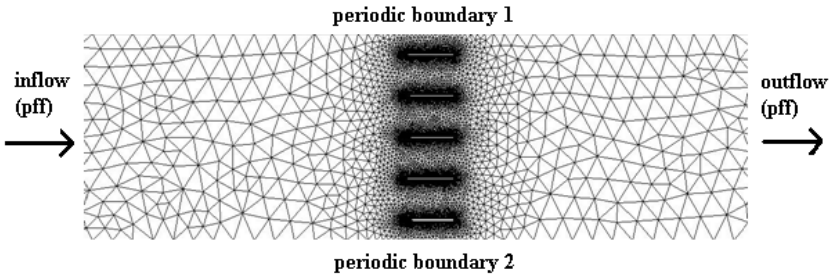

Figure 2.5: Domain definition and the computational grid in the 2-D study

A series of CFD solutions are conducted at sea-level atmospheric conditions and in a range of Mach numbers centered at $M = 0.80$. The commercial CFD package of FLUENT is utilized in this study. Local Mach number data are collected at two points on the mid-line between one pair of parallel plates. The first data point is located in upstream and distance between this point and the plates is approximately three chord length of plates. The other data point is located at the exit. The results at the upstream and exit of fins are examined to identify the variation of local Mach number along the mid-line. It should be noted that, it is not possible to set M_∞, i.e. Mach number at the inflow and outflow boundaries of this problem. As a result of characteristic relations at the

subsonic inlet/farfield boundaries, the physical boundary condition is given as

$$v_n + \frac{2a}{\gamma + 1} = \text{const.} \tag{2.6a}$$

and numerical boundary condition is

$$v_n - \frac{2a}{\gamma + 1} = \text{const.} \tag{2.6b}$$

where v_n and a are the normal velocity component and speed of sound at the boundary, respectively [35]. This shows that, for a given initial condition, speed of sound, and hence Mach number at the boundary are settled as the conditions given in Eq. 2.6 are satisfied.

CFD results show that local Mach number at the fin exit, M_e, does not exceed 1.0, and local Mach number at throughout upstream region of parallel plates, M_u, does not exceed 0.79, even if specified initial value for M_∞ is increased up to 0.93 (see Fig. 2.6). $M_e = 0.79$ is considered as a quite close value when compared to the design Mach number value of this study, which is 0.80. Although these solutions does not represent the whole physics of the problem, it certainly supports the idea of similarity between the behavior of a grid fin cell and a converging nozzle.

2.2.3 Grid Fin in Supersonic Flight

A grid fin in supersonic flight is exposed to shock waves in different patterns, depending on the Mach number of the flow. For the Mach numbers that are slightly larger than 1.0, a bow shock occurs in front of the leading edges of the grid fin (see Fig. 2.7a) [7]. This is also referred to as a detached shock. As Mach number is increased, location of the shock gets closer to leading edges of the fin. At a certain Mach number value shock waves become attached to leading edge, as seen in Fig. 2.7b. After this threshold, oblique shock and rarefaction waves are observed in case of any change in direction of the air flow. Oblique waves reflect from the walls of the grid fin at relatively low Mach number values. With further increase in Mach number, oblique shock angles become narrower, thus, they turn into non-reflecting waves, as shown in Fig. 2.7c.

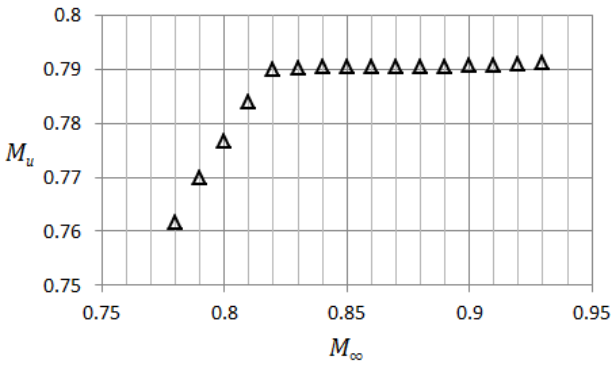

(a) Upstream local Mach number

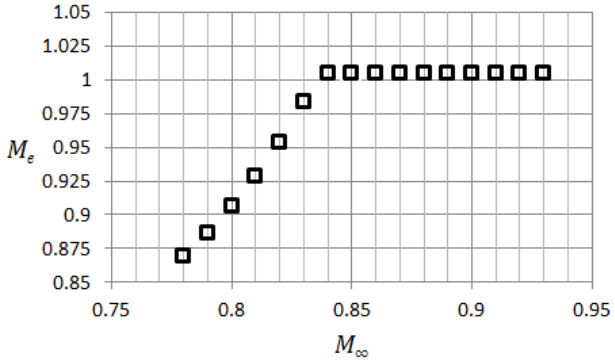

(b) Fin exit local Mach number

Figure 2.6: Results of 2-D CFD study for flow between parallel plates

Shown in Fig. 2.8 represents the reflecting and non-reflecting wave patterns over a grid fin schematic. Flow with an angle of attack creates a lift force on each surface of this, by pressurizing region 1 and depressurizing region 2, in both schemes. However, in case of reflecting wave pattern (on the left), expanded air region 3 and compressed air region 4 result in a decrease in lift force. As a result of this assessment, a grid fin with a non-reflecting wave pattern is considered as a requirement for a suitable design.

2.3 Critical Mach Numbers

The grid fin flow regimes introduced and explained in Section 2.2 are separated by definite Mach number thresholds, called 'critical Mach numbers' by Belot-

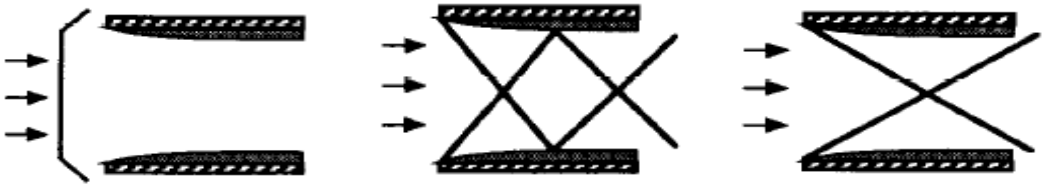

(a) Detached shock wave (b) Reflecting waves (c) Non-reflecting waves

Figure 2.7: Supersonic phenomena occurring within a grid fin [36]

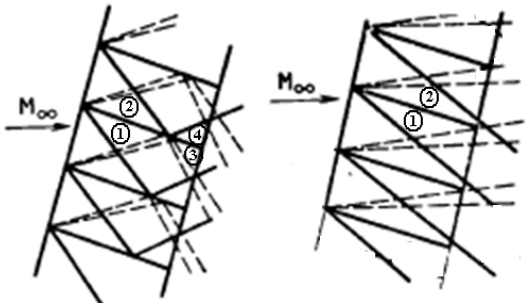

Figure 2.8: Pressure regions within a grid fin (changed from Ref. 7)

serkovsky *et al.* [7]. These are abbreviated as M_{cr1}, M_{cr2} and M_{cr3}.

The first critical Mach number, M_{cr1}, is defined as the minimum value at which the flow inside the fin is choked. It is calculated, for a specific grid fin geometry, by solving Eq. 2.1 for M_∞. Isentropic flow tables [33, 37] are also useful for this purpose. It should be pointed out that M_{cr1} is always lower than unity. Grid fins operating in the freestream Mach number range $M_{cr1} < M_\infty < 1$ are exposed to choking.

Bow shock, which occurs at very low supersonic Mach numbers, is theoretically attached to leading edges of grid fin at the second critical Mach number, M_{cr2}. Value of this number is calculated by solving the second root of the same equation as done in calculation of M_{cr1} [7]. Isentropic flow tables are also useful for this parameter, too. M_{cr2} is always larger than unity.

For the Mach numbers larger than M_{cr2}, oblique shock and rarefaction waves are observed in flows with angle of attack. In flows with no angle of attack, these waves turn into infinitesimal perturbations aligned with Mach lines, which are inclined by the Mach angle, μ, with grid fin walls. By definition, at freestream

Mach number higher than or equal to M_{cr3}, Mach lines do not reflect from the grid fin walls, as shown in Fig. 2.9. Therefore, grid fins operating in freestream Mach number range $M_{cr2} < M_\infty < M_{cr3}$ experience reflecting waves. For a specific grid fin geometry, the third critical Mach number, M_{cr3}, is calculated by the graph shown in Fig. 2.10.

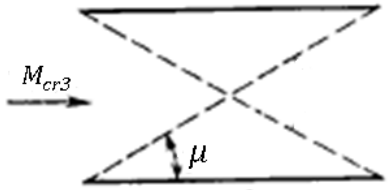

Figure 2.9: Definition of M_{cr3} [7]

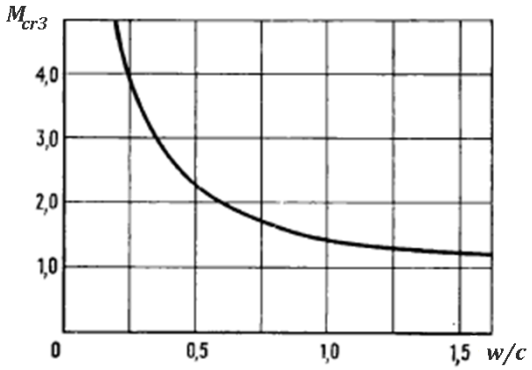

Figure 2.10: Calculation of M_{cr3} [7]

In the light of these explanations, Table 2.1 summarizes the flow regimes over a grid fin with their freestream Mach number conditions. Choked flow, bow shock and reflecting wave regimes are attributed as problematic and designers should avoid such kind of grid fin designs. In this thesis, it is aimed to design a grid fin having subsonic flow characteristics at a design Mach number within transonic range of speeds.

Table 2.1: Grid fin flow regimes

Flow regime	**Lower bound (M_∞)**	**Upper bound (M_∞)**
Subsonic	0	M_{cr1}
Choked flow	M_{cr1}	1
Bow shock	1	M_{cr2}
Reflecting wave pattern	M_{cr2}	M_{cr3}
Non-reflecting wave pattern	M_{cr3}	∞

CHAPTER 3

METHODOLOGY

In this chapter, a design process developed for grid fin controls is explained. The procedure aims to determine appropriate geometric properties of grid fin, definitions of which are introduced in Section 2.1, in pre-defined flight conditions, which is referred to as design conditions.

Grid fin is composed of planar surfaces repeating themselves in a pattern. This allows reducing the computational domain into smaller representative portions, which are called "unit" cells. This concept is introduced in current thesis study. Conducting the design efforts and making assessments on unit grid fin is reasonable for being economic in spending time to generate a geometric model and computational grid as well as to carry out computations. A schematic of the unit grid fin (UGF) is shown in Fig. 3.1. Shaded region can be used as the fluid domain in computations.

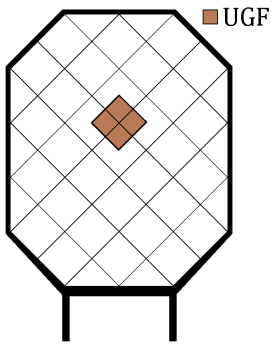

Figure 3.1: Unit grid fin representation

3.1 Description of the Computational Method

Computational Fluid Dynamics (CFD) is the major method to predict the aerodynamic forces exerted on grid fin and missile body surfaces. 'Unit grid fin' approach is employed to make solutions simple and to ensure flexible design.

CAD models are created in ANSYS Design Modeler package. Parametric design option is helpful in reproducing the models of different dimensional properties. Cylindrical enclosure volume, which has minimum ∼20 times greater diameter and length dimension, is created to represent the flow domain. The aerodynamic model is located at the center of enclosure volume (see Fig. 3.4).

ANSYS 14.0 meshing tool and Tgrid 5.0 is employed to generate unstructured grids. For all geometric configurations of missile and grid fin geometry, surface mesh consists of triangular elements in order to ease the production of high quality cells. Prism layers are grown starting from the surface for the purpose of resolving the high velocity gradients in boundary layer. In order to fill the remaining volume of the domain, tetrahedral cell elements are generated. As a result, computational domain is composed only of wedge and tetrahedral cells.

Pressure-based Reynolds Averaged Navier-Stokes solver of FLUENT 14.0 is utilized throughout the study [38]. Ideal gas assumption is selected as equation of state for air flow. Viscosity-temperature relation is characterized by Sutherland's law. One equation Spalart-Allmaras model is utilized as the turbulence model. Momentum and energy equations are discretized by second order upwind scheme in order to obtain more accurate drag results. Coupled algorithm of FLUENT solver is employed to make the simulations converge faster.

3.2 Validation of the Computational Method

In this section, validity of the computational model is tested and possible sources of error are stated.

3.2.1 Agreement with Experiment

Wind tunnel tests of various grid fin designs were conducted by Washington and Miller [14]. Aerodynamic forces and moments on grid fin was measured while it was being mounted on an ogive nose 10.4 caliber long cylindrical missile body (see Fig. 3.2). Four grid fins were placed in (+) configuration. The balance was located between missile body and fin number 4, in order to measure the aerodynamic loads on the fin alone. Fin normal force measurements in angle of attack (α) sweep range $[0°, 15°]$ at Mach numbers 0.7, 1.2 and 2.5 are of interest in this validation study.

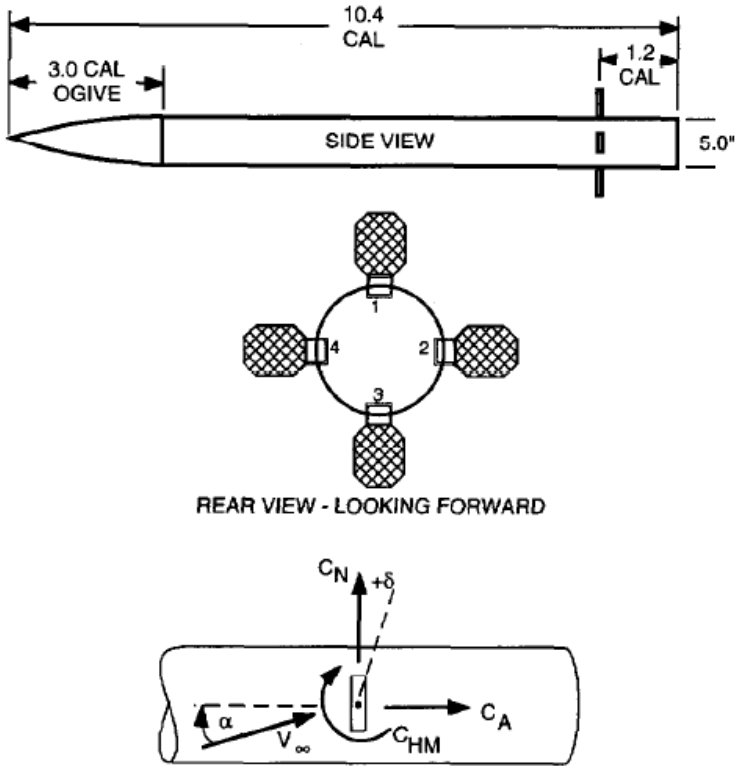

Figure 3.2: Model and sign conventions of wind tunnel test [14]

Air flow over a missile with grid fins model of the same dimensions as in the Washington & Miller's study [14] is computed and normal normal force variation with the increasing angle of attack on the fin number 4 is observed. The configuration designated by 'G12' in Ref. 14, whose technical drawing is presented in Fig. 3.3, is used for validation case. The solution matrix is composed of angle

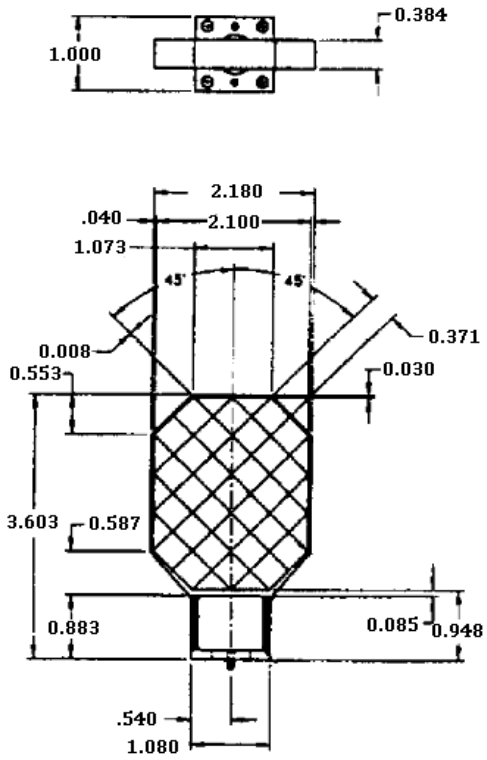

Figure 3.3: Technical drawing of G12 (Dimensions are in inches)

of attack values 2.5°, 5.0°, 7.5°, 10.0°, 12.5°, 15.0°and of Mach numbers 0.7, 1.2, 2.5.

Outer surfaces of enclosure domain (see Fig. 3.4a) is assigned as pressure-far-field boundary condition allowing to input Mach number, flow direction, static pressure and static temperature. Pressure and temperature values are taken as standard sea-level conditions ($p_\infty = 101325$ Pa, $T_\infty = 288.15$ K). No slip wall boundary condition is assigned to missile body and grid fin surfaces seen in Fig. 3.4b. Initial values before starting iterations for every cell in the domain are taken from the quantities assigned on pressure-far-field surfaces.

The mid-section of volume mesh and surface mesh on one of the grid fins are shown in Fig. 3.5. Surfaces of grid fins are finely resolved to ensure sufficient resolution without spending any effort to grid independence work. Surface mesh independence for very similar geometries is verified in Chapter 4 with much coarser grids. Number of triangular surface elements is 2,262,930. After 8 layers of prisms and tetrahedral volume elements are generated, 31,261,800 cell ele-

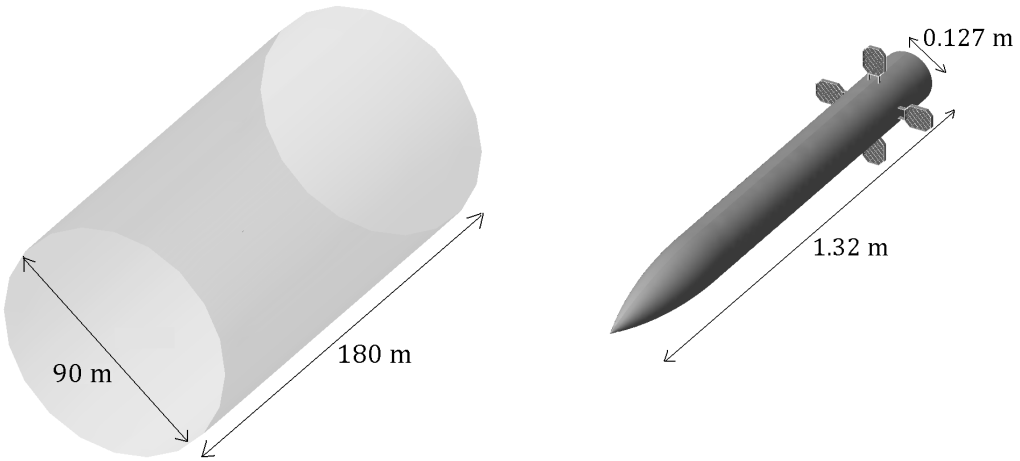

(a) (b)

Figure 3.4: Enclosure and missile geometries

ments in total are obtained. Prism layers are grown by specifying constant first layer thickness and constant last layer aspect ratio. The values of these parameters are 10^{-5} m and 4.0, respectively. The dimensionless wall distance for the first layer thickness is kept below $y^+ = 5$ for most of the surfaces, to ensure that the first prism layer is located within the viscous sublayer [38] (see Fig. 3.6a-c-e). It is also seen that the total thickness of prism layer is capable of resolving the whole boundary layer by analyzing the velocity vectors qualitatively. Those in the last prism layer are of the same size as the external velocity vectors, as seen in Fig. 3.6b-d-f. The screenshots are taken in a plane perpendicular to grid fin surface.

Aerodynamic normal force on the right hand side grid fin (fin number 4 in Fig. 3.2) is calculated by evaluating surface integral of static pressure and viscous drag contribution. The force values are non-dimensionalized by normalizing with dynamic pressure and reference area, which is the cross-sectional area of the missile body.

$$CN = \frac{N}{\frac{1}{2}\rho V^2 S_{ref}} \tag{3.1a}$$

or, equivalently,

$$CN = \frac{N}{\frac{1}{2}\gamma p M^2 S_{ref}} \tag{3.1b}$$

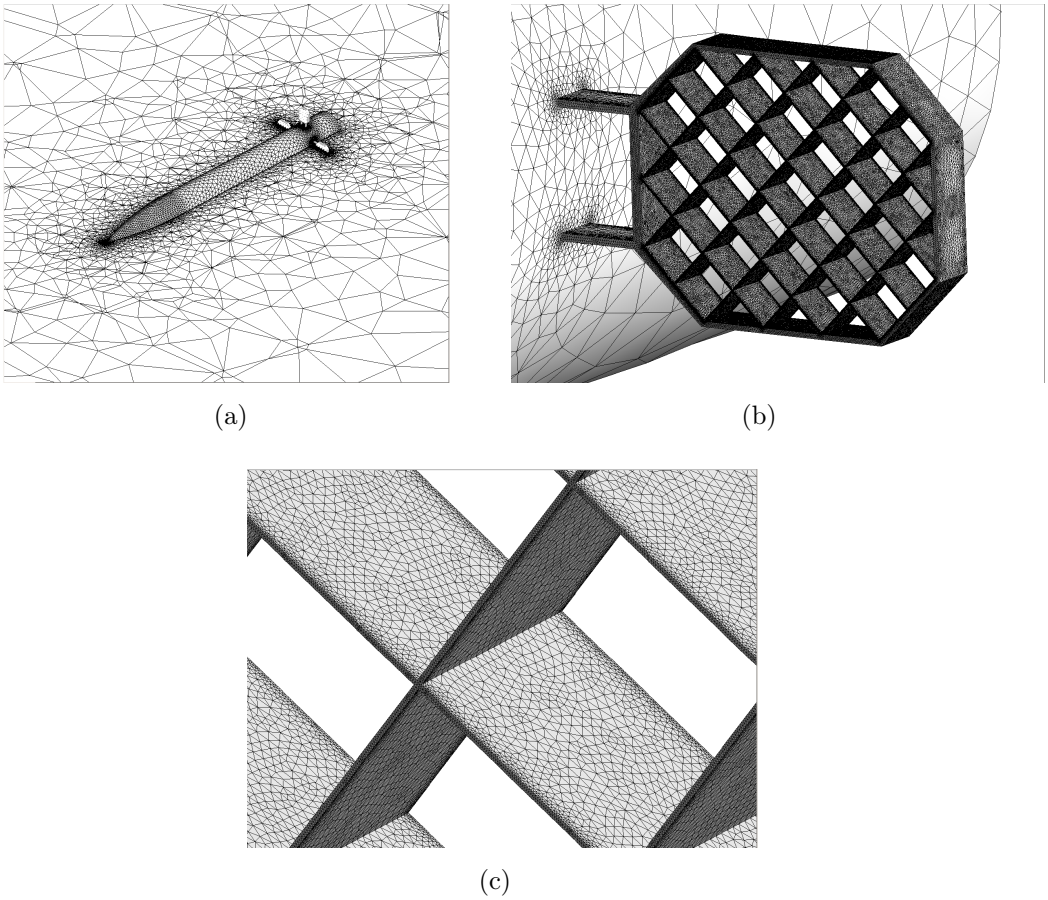

(a) (b)

(c)

Figure 3.5: Volume and surface meshes used in computations

Normal force comparison with the experiment is made in three distinct flight regimes. Agreement between density-based and pressure-based solutions shows the algorithm independence (see Fig. 3.7); therefore, the latter is possible to be used in this compressible flow problem with a satisfactory accuracy. Pressure-based algorithm is preferred for its stability and faster convergence. When the CFD solutions are compared to the experimental data, a good agreement is seen in the normal force coefficient within the wide range of Mach numbers (see Fig. 3.7). Maximum relative error is observed as 10% among all cases.

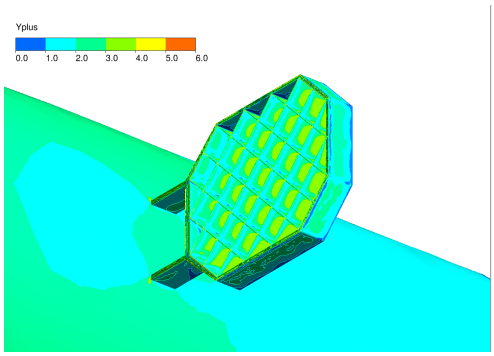

(a) y^+ contours ($M = 0.7$)

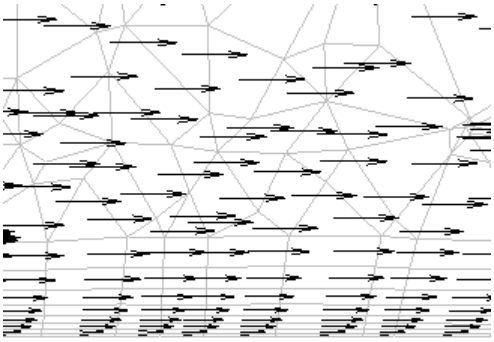

(b) B.L. velocity vectors ($M = 0.7$)

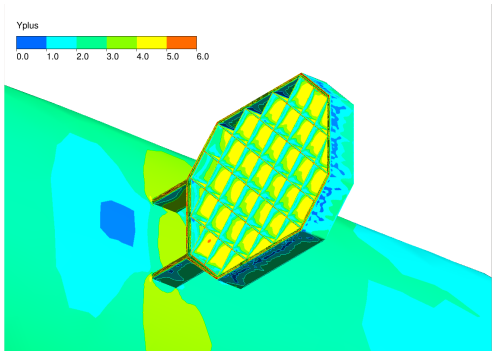

(c) y^+ contours ($M = 1.2$)

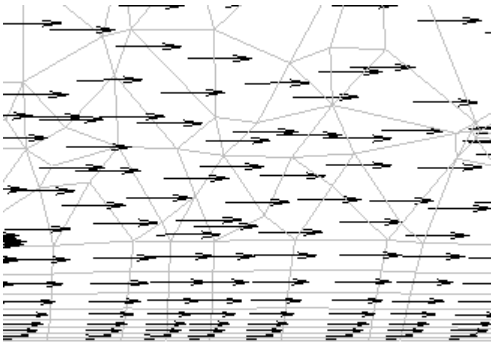

(d) B.L. velocity vectors ($M = 1.2$)

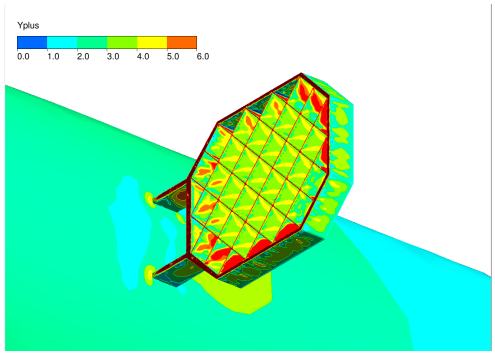

(e) y^+ contours ($M = 2.5$)

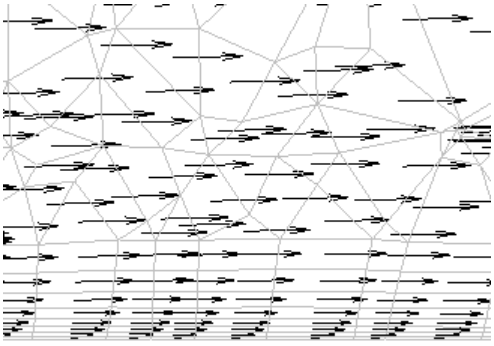

(f) B.L. velocity vectors ($M = 2.5$)

Figure 3.6: Boundary layer resolution inspection

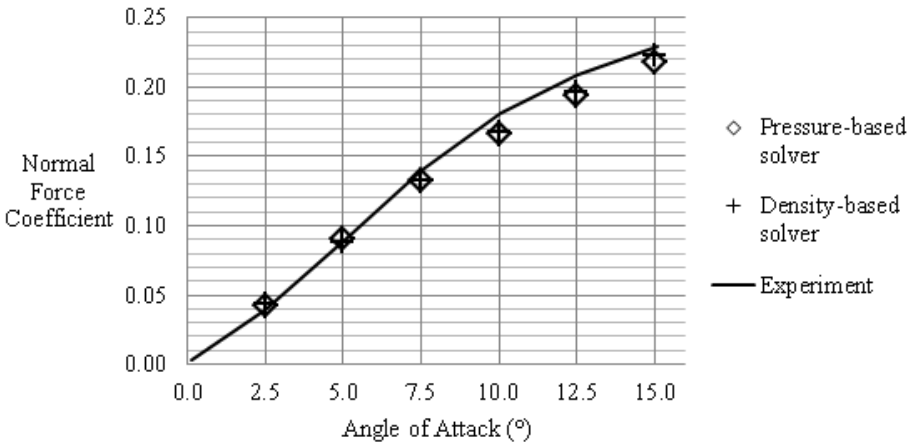

(a) M=0.7

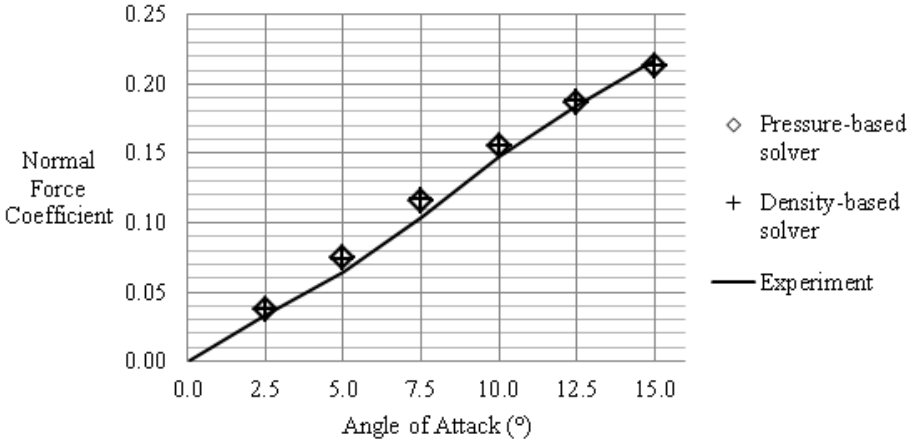

(b) M=1.2

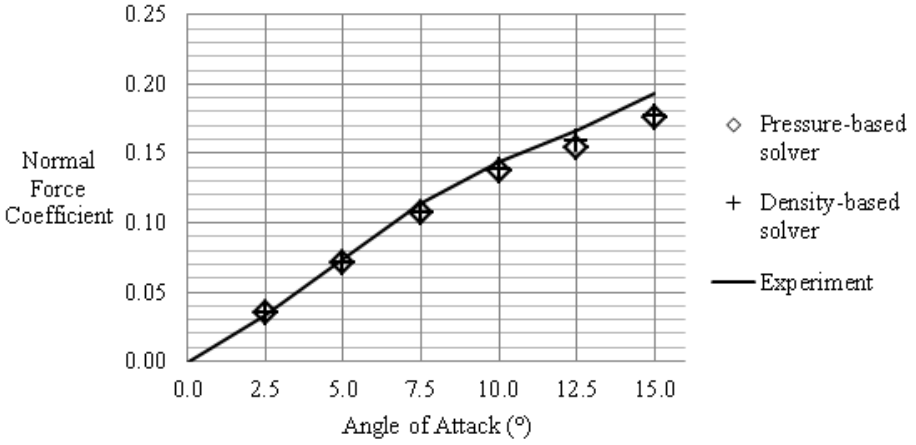

(c) M=2.5

Figure 3.7: Comparison between CFD solutions and the experiment of Washington & Miller

3.2.2 Effect of Missile Body

CFD solutions are to be carried out to characterize the flow field around the unit grid fins. By doing this, it is aimed to acquire representative data for whole grid fin. However, missile body effect on the flow field is not modeled in this method. This reality comes with a requirement of information about the effect of missile body on grid fin performance. In order to understand the contribution of body, validation study in Section 3.2.1 is repeated with grid fins isolated from body.

In isolated grid fin case, exactly the same surface mesh is employed. The fin takes place in the flow alone, as shown in Fig. 3.8b. Comparison with the 'on body' case (shown in Fig. 3.8a) enables observing the changes in the flow field,

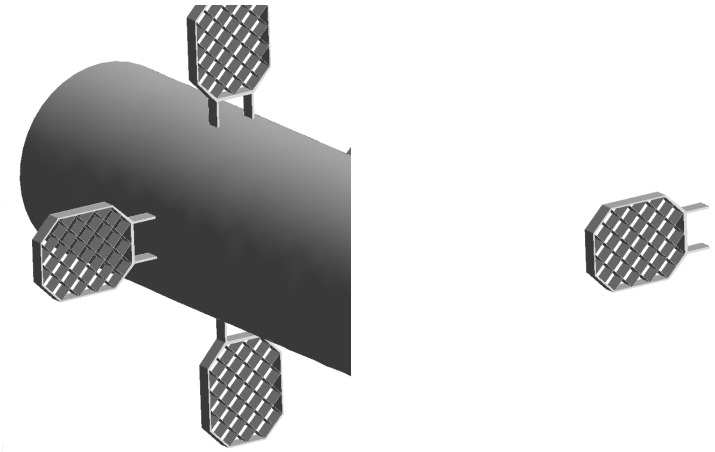

(a) (b)

Figure 3.8: 'Grid fin on body' (a) and 'isolated grid fin' (b) cases

as well as their outcomes on the aerodynamic properties.

Normal force comparison of the isolated grid fin with that attached on missile body shows that there is a significant amplifying effect of the body. The reason for that is, so called, upwash effect, observed around side regions of a slender object exposed to an air flow with an angle of attack. Upwash effect brings an increase in effective angle of attack of side grid fins. On the contrary to the those placed on sides, upper and lower fins are encountered by a downwash, which lowers the local angle of attack in those regions. Fig. 3.9, which represents

the solution at $M = 0.7$ and $\alpha = 2.5°$, illustrates the up- and downwash effects due to the existence of a body on the transverse plane immediately upstream of grid fins. A dimensionless parameter $K = \dfrac{\alpha_{eff} - \alpha}{\alpha}$ is defined to quantify the magnitude of angle of attack deviation. In this definition, effective angle of attack is calculated from the local velocity component data in principal body axes: $\alpha_{eff} = \tan^{-1}(\frac{w}{u})$, where u and w are the velocity components in x- and z-directions, respectively. Positive values of K indicate upwash.

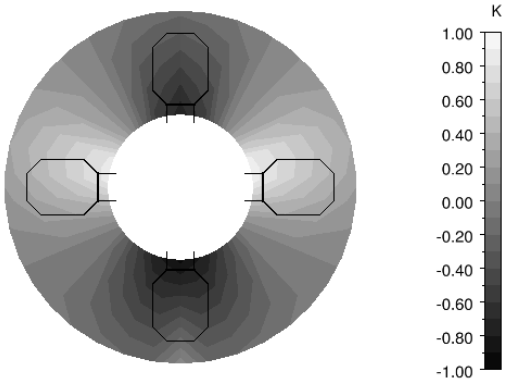

Figure 3.9: Variation of coefficient 'K' in upstream of grid fins

Side fins are exposed to a higher local angle of attack than the missile body. This creates a difference between aerodynamic forces 'on body' and 'isolated' models. Therefore, a correction is required if the normal force of grid fin is computed using an isolated model. For this purpose, previous work can be employed to obtain a consistent data in absence of missile body in the computational model. Interaction between components of an air vehicle was studied in a NACA report [39] and it is reported that the variation of effective angle of attack in the horizontal symmetry plane obeys the relation 3.2. In equation 3.2, r and y denote the missile body radius and distance from centerline of the missile body, respectively. Effective angle of attack of side grid fins can be approximated with the local angle of attack in the horizontal symmetry plane. It should be noted that the coefficient 'K' decreases in magnitude as moving away from the body. Therefore, the effective angle of attack of grid fin is not a constant, rather, it decreases in spanwise direction.

$$\alpha_{eff} = \alpha(1 + \frac{r^2}{y^2}) \tag{3.2}$$

Normal force curves obtained by the 'on body' and 'isolated' models show significantly different slopes, as seen in Fig. 3.11. The reason for this is the issue discussed in previous paragraphs. When a correction factor is applied on the outcome of the 'isolated' model, a good agreement is attained. The correction factor is determined using mean effective angle of attack of grid fin. This is calculated by taking average of effective angle of attack between both ends in spanwise direction.

$$\overline{\alpha_{eff}} = \frac{1}{y_2 - y_1} \int_{y_1}^{y_2} \alpha_{eff} dy \tag{3.3}$$

inserting Eq. 3.2, the integral in Eq. 3.3 is evaluated as

$$\overline{\alpha_{eff}} = \alpha(1 + \frac{r^2}{y_1 y_2}) \tag{3.4}$$

Mean effective angle of attack is calculated by above relation for the validation problem and the normal force coefficient curve is corrected by the factor $\frac{\overline{\alpha_{eff}}}{\alpha}$ due to the linear nature of the aerodynamic normal force. Therefore, correction factor 'f' is expressed as:

$$f = 1 + \frac{r^2}{y_1 y_2} \tag{3.5}$$

Placement of the grid fins on the missile body is schematically expressed in Fig. 3.10. When these dimensions are substituted into Eq. 3.5, correction factor, f, is obtained as 1.34. Further, data calculated for isolated grid fin are multiplied by the correction factor and satisfactory agreement with the results of fin attached on body is achieved at $M = 0.7$ and $M = 1.2$. At high supersonic speeds, curves follow each other up to 10°angle of attack but beyond that value, result starts to deviate, as shown in Fig. 3.11.

3.2.3 Validity of 'Unit Grid Fin' Approach

A grid fin is composed of a rectangular pattern of surfaces of the same dimensional parameter values. Therefore, the unit grid fin (UGF) concept, which was mentioned at the beginning of this chapter, is introduced here. To reduce the computational efforts, use of UGF models is advisable. However, it is required

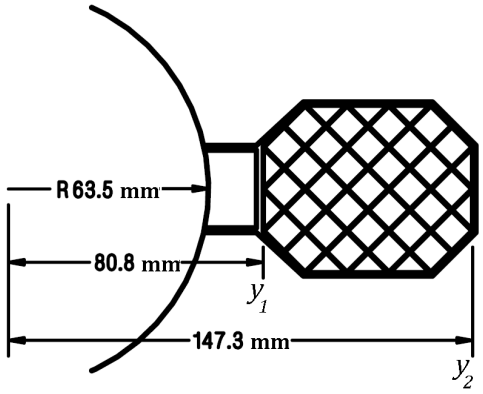

Figure 3.10: Placement of grid fin on missile body in CFD solutions

to know how well it represents the actual flow domain. For this reason, in this section, validity of this approach is checked as a part of validation campaign.

It is argued that aerodynamic loads on a grid fin can be calculated through the computation of forces and moments on UGF and multiplication with the 'number of repetitions', 'n', i.e., the number of UGFs comprising the grid fin. Therefore, components other than internal framework, such as external frame and connection rods to missile body, are not taken into consideration. In other words, by employing the current method, only the loads on internal framework can be inferred. Therefore, aerodynamic force results obtained by UGF computations are to be compared to those on internal surfaces of full GF model (see Fig. 3.12).

The flow field around UGF is computed using a domain consistent with the full model described in Sections 3.2.1 and 3.2.2. Dimensions of chord, width and thickness are preserved as shown in Fig. 3.13. Lateral boundaries of the domain are assigned as periodic boundaries. Inflow and outflow is provided by non-reflecting pressure-far-field type of boundary condition (see Fig. 3.14), allowing the user to specify Mach number and direction of the flow, so that the desired flow speed and angle of attack and/or angle of sideslip are assured. The distance between the two far-field boundaries is 20 times the chord length (194 mm).

Number of repetitions, n, is determined by counting the number of 'nodes' (shown in Fig. 3.15), i.e., intersection lines of surfaces of cross-shaped UGFs. UGF has four surface pairs similar to each interior node and it exactly matches

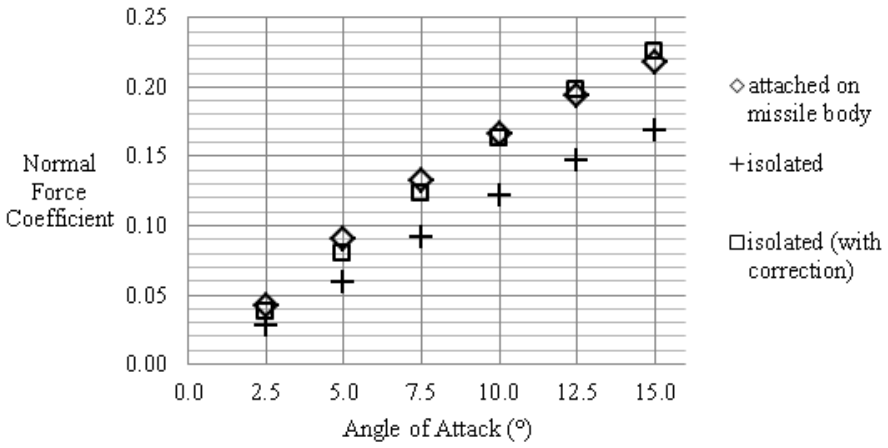

(a) M=0.7

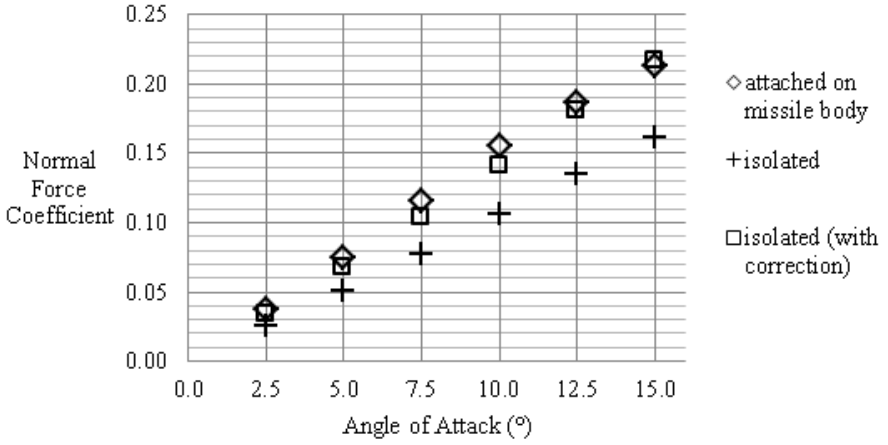

(b) M=1.2

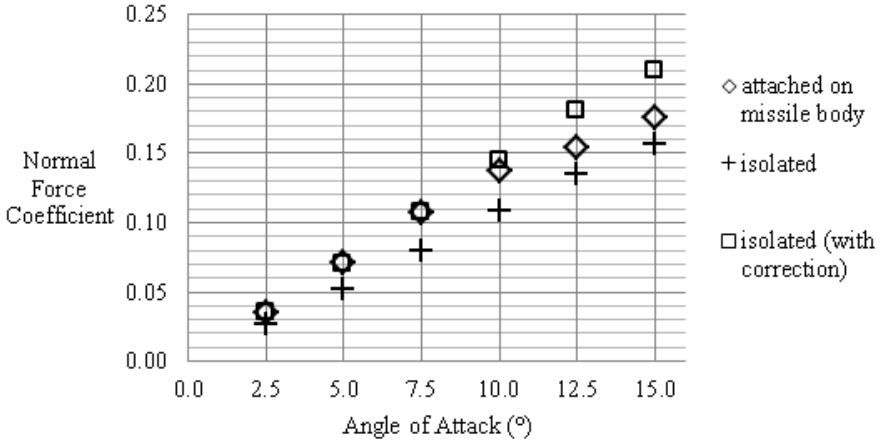

(c) M=2.5

Figure 3.11: Comparison of normal force coefficients of grid fin in attached and isolated configurations

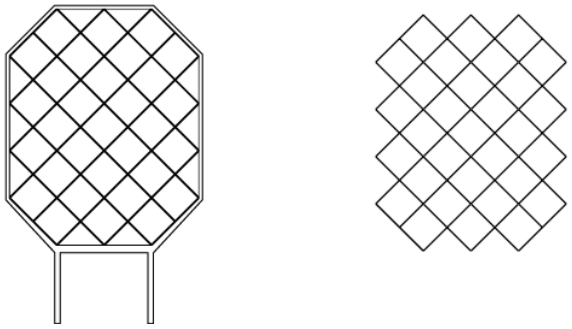

(a) (b)

Figure 3.12: The real GF model (a) and internal surfaces used in comparison with UGF (b)

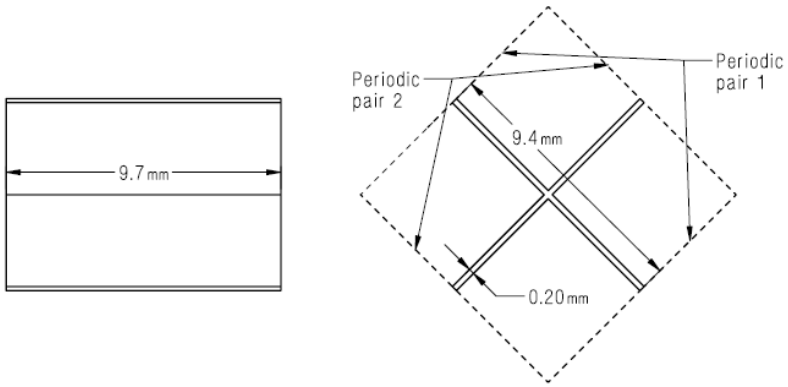

Figure 3.13: UGF model and its geometric properties

with a great majority of the GF nodes. These nodes are designated as of type 1. Although a great portion of grid fin is covered by the first type nodes, side and corner nodes have three and two extensions, as shown in Fig. 3.15, respectively. Therefore, they are designated by type 2 and type 3.

Once the total lifting surface area of extensions of the node types are considered, it is understandable that surfaces of type 1 nodes act as a full UGF, while those of type 2 and of type 3 nodes represent $^3/_4$ and $^1/_2$ of a UGF, respectively. When the number of repetitions is counted in this manner, 28 of type 1, 4 of type 2 and 14 of type 3 nodes are detected and this corresponds to 38 UGF in total. Therefore, aerodynamic loads on UGF should be multiplied by 38 to make a proper comparison between internal faces of GF and UGF.

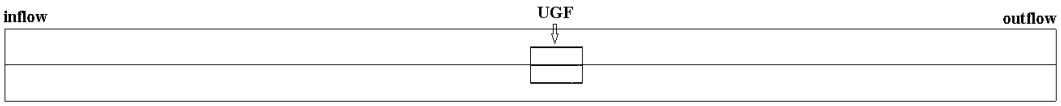

Figure 3.14: Domain schematic of UGF model

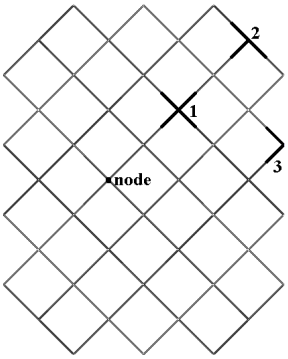

Figure 3.15: Node types in the GF

Comparison between the normal force on internal surfaces of the GF model and that on 38 UGF is shown in Fig. 3.16. In this figure, it is understood that the current UGF method provides superior prediction performance in subsonic and high supersonic speed ranges with a good agreement. Therefore, the validation of the use of UGF models has been completed for these regimes. However, designer should be careful in using the method in low supersonic speeds ($\approx$1.2), due to significantly different slopes obtained by the two solutions. It should be noted that this Mach number is most probably in the interval of normal shock regime of flow around GFs, which was introduced by Belotserkovsky *et al.* [7] as such that a normal bow shock forms in front of the leading edge when the flow Mach number is less than the 'second critical Mach number'. This creates a difficulty in computing such an abruptly changing flow field by utilizing a tube-like computational domain surrounded by periodic surfaces. This issue could be studied in the future and be converted to a more accurate method in low supersonic range of speeds.

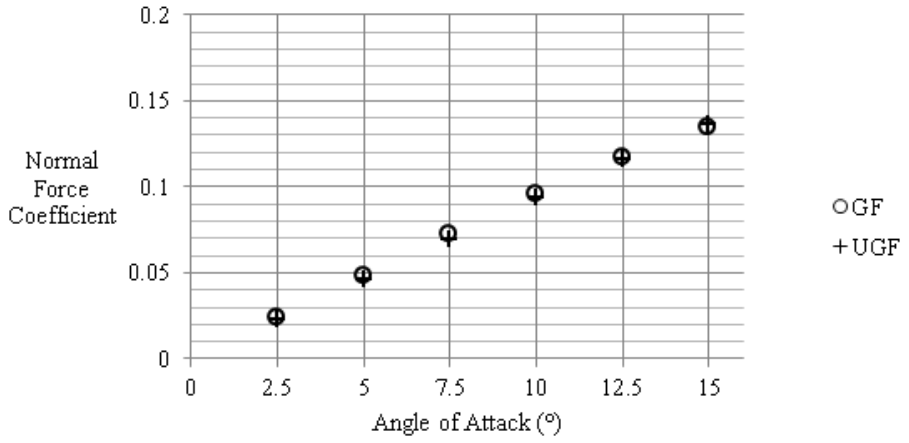

(a) M=0.7

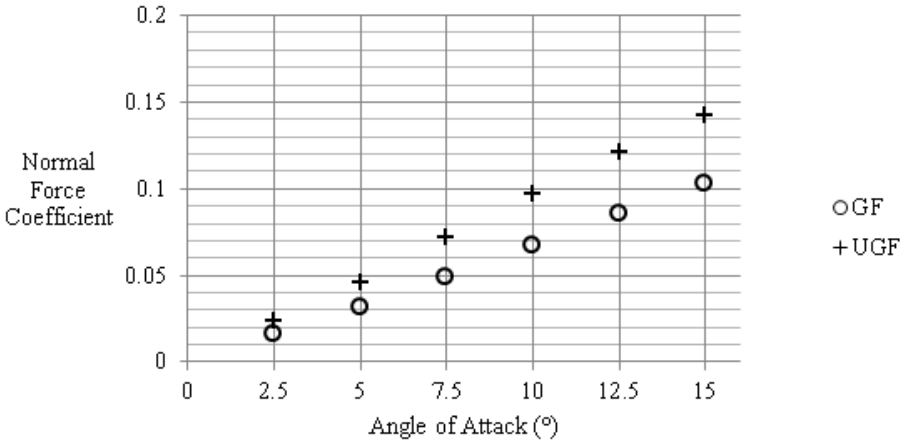

(b) M=1.2

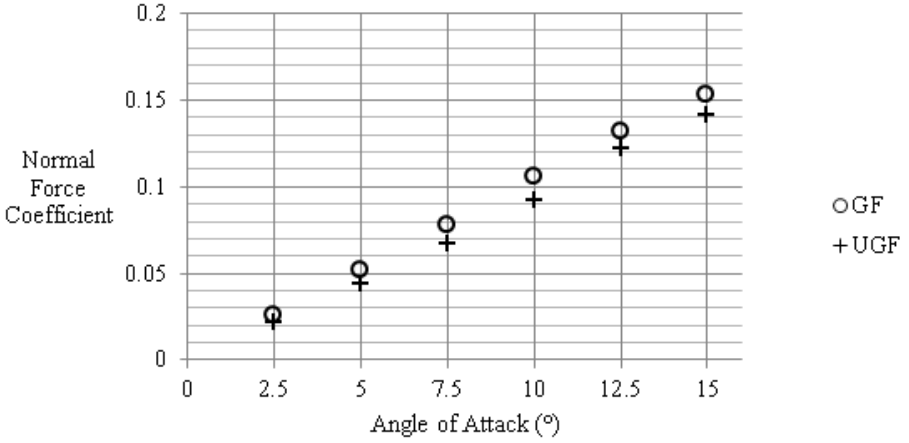

(c) M=2.5

Figure 3.16: Normal force comparison of 38×UGF model and internal surfaces of GF

3.2.3.1 Mesh Independence of UGF Solutions

The mesh independence study for UGF solutions is carried out by changing the grid resolution in leading and trailing edges of the model, around which the highest pressure gradient values take place. The simulations are conducted at $M = 0.7$, which is of the main concern in this thesis. In order to observe the normal force on the wall surface of unit grid fin, a non-zero angle of attack of $\alpha = 5°$ is selected as the flow condition.

For the mesh independence check, trailing and leading edge surfaces are divided into 6 and 10 lines which are composed of triangular face elements. Sizes of grid elements in a section plane are shown in Fig. 3.17.

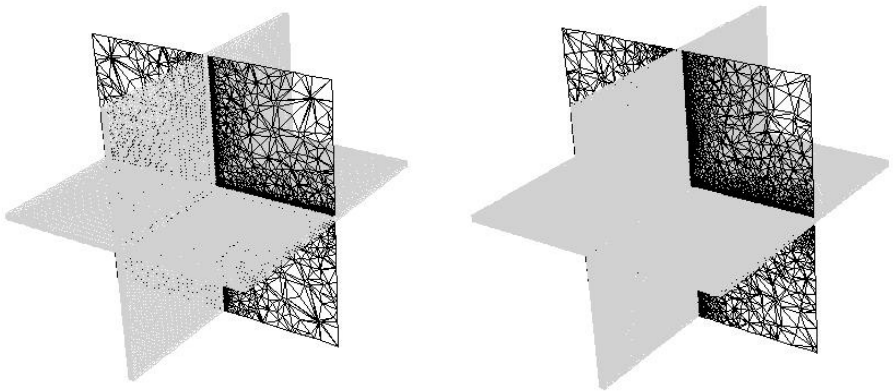

(a) Coarse (b) Fine

Figure 3.17: Different grid resolutions used in mesh independence study

Normal and drag force values obtained by using each grid are presented in Table 3.1. The pressure contours within the upper and lower surfaces are shown in Fig. 3.18. Considering the results, it is concluded that the coarse grid performs more than enough in determination of normal force. Drag force accuracy is also accepted as sufficient, because quantitative accuracy in prediction of drag is not as important as that of normal force in design of a grid fin.

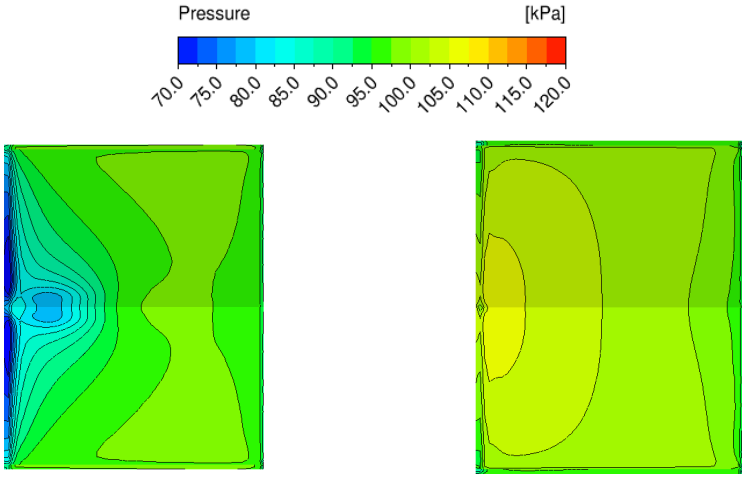

(a) Coarse grid (top surfaces)

(b) Coarse grid (bottom surfaces)

(c) Fine grid (top surfaces)

(d) Fine grid (bottom surfaces)

Figure 3.18: Pressure contours obtained in the mesh independence study

Table 3.1: Comparison of force components obtained by coarse and fine grids

	# of surface elements	**Normal force**	**Drag force**
Coarse	41,344	84.16 N	18.09 N
Fine	134,624	83.98 N	17.61 N
Difference		0.2%	2.7%

3.3 Fundamental Considerations in Design of a Grid Fin

Design procedure aims to arrange an effective configuration of grid fins in terms of aerodynamic stability and control. This is ensured by creating sufficient amount of moment about center of gravity of a missile. In this design process, longitudinal static stability and pitching moment control are of interest.

For a stable missile, pitching moment must be in counter direction of angle of attack. Therefore, signs of moment coefficient and angle of attack must be negative of each other in case of an axisymmetric missile body. In general, the stability parameter, which is change in pitching moment coefficient with respect to angle of attack, Cm_α, has a negative value for stable missiles. The higher magnitude of this parameter, the stronger static stability.

$$Cm_\alpha = \frac{\partial Cm}{\partial \alpha} < 0 \tag{3.6}$$

Longitudinal control of a missile is performed by means of pitching moment created by deflection of grid fin control surfaces. The change in pitching moment coefficient with respect to elevator angle, $Cm_{\delta e}$, is linear in nature within a few degrees of rotation. By definition, positive deflection angle yields a positive moment, therefore,

$$Cm_{\delta e} = \frac{\partial Cm}{\partial \delta e} > 0 \tag{3.7}$$

Control characteristics of a missile is generally influenced by Cm_α and $Cm_{\delta e}$ parameters. As high Cm_α implies a strong stability, maneuverability of such missiles is negatively affected due to the high moment requirement for a certain value of angle of attack. As a result, strength of pitch control is not only a function of $Cm_{\delta e}$. Instead, a new parameter, pitch control effectiveness, is in-

troduced as $\frac{\alpha}{\delta e} = \frac{Cm_{\delta e}}{Cm_{\alpha}}$, which expresses, roughly, how much deflection angle is required to obtain a certain angle of attack value. Fleeman recommends this value to be greater than 1 for all kinds of tactical missiles [3].

Drag coefficient, CD, is the other parameter that is to be taken into consideration in design procedure. Drag force is considered as a loss in most of the air vehicle system design efforts. Therefore, the drag contribution of grid fin in overall missile drag should be minimized in order to obtain an efficient control device. Drag force is mainly dependent on the cross-section, area of which is driven by the thickness parameter. As a result, this parameter should be arranged as thin as manufacturing and operating conditions allow.

Overall dimensions of the design should be taken as one of the considerations in evaluation of the design alternatives. Design efforts should also aim at a manufacturable, utilizable and maintainable solution.

When the design procedure is concerned with the help of these arguments, the first step is suggested to be determination of an objective goal for a missile with grid fin. Pitch control effectiveness is considered as the strongest candidate for its importance in expressing the maneuverability of the missile. In this case, a specific $\frac{\alpha}{\delta e}$ value might be selected as the design objective. As well as serving as control devices, fins are essential means of stability. Hence, the designer might be subject to choosing the stability parameter, Cm_{α}, to ensure a certain level of longitudinal static stability.

Neither of design objectives mentioned up to this point can lead to a unique configuration in design space. That is, more than one geometric configurations are probably able to satisfy the requirement of the design objective. Details of this issue is to be explained in the sample design performed in Chapter 4. For this reason, designer is required to figure out the most efficient solution, which is, in this study, prescribed as the minimum drag alternative.

3.4 Assessment on Fin Arrangement

Throughout the thesis, four fin missile configurations are considered, although three or more fins can also achieve static stability and control [3]. In general, independent of whether they are planar and grid fins, the four fins are arranged in two distinct configurations: + (plus) and × (cross). Both alternatives are utilized for stability and control purposes when the fins are located at the rear of the flight vehicle.

The three basic moment components about the principal axes of a missile can be generated using + or × configured fins. Fig. 3.19 shows the use of one of the most effective fin sets in order to perform each of the roll, pitch and yaw maneuvers in their positive direction. Arrows indicate the direction towards which leading edges of related fins move.

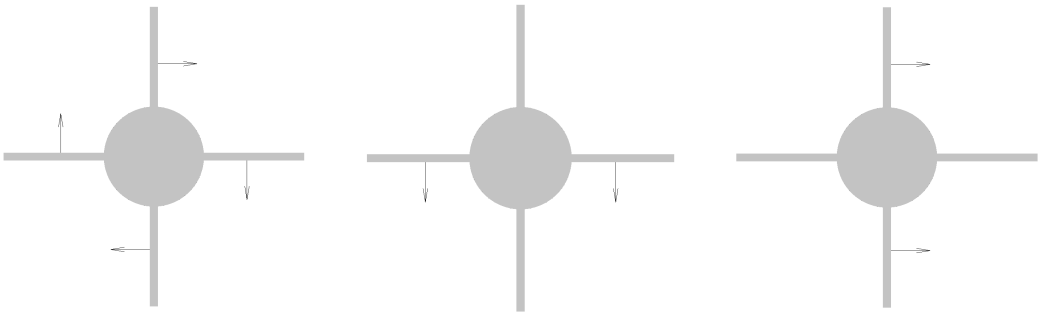

(a) Roll (+) (b) Pitch (+) (c) Yaw (+)

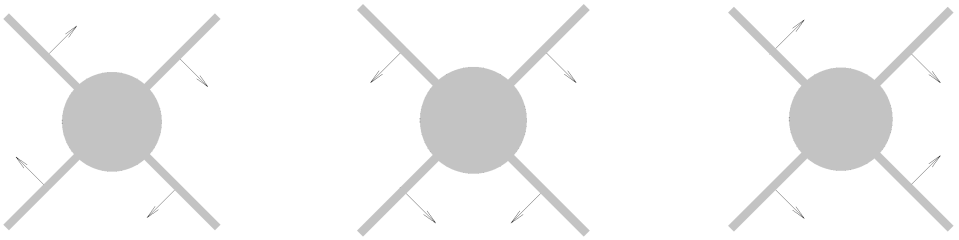

(d) Roll (×) (e) Pitch (×) (f) Yaw (×)

Figure 3.19: Maneuvering by + & × fin arrangement configurations (Figures are of back view.)

In case of + configuration, only two fins are active in pitching and yawing maneuver, while all fins are dynamic when × configuration is used. Similarly, when pitch and yaw stabilities are considered, two fins stabilizes a +-configured missile having planar fins. On the contrary, all four fins contribute to stability of a ×-configured missile. Therefore, control effectivenesses of the two is concluded to be comparable, in case planar fins are utilized.

Contrary to planar fins, in case of use of grid fins, all four fins has a contribution to pitch and yaw stability, regardless of their arrangement. Nevertheless, aerodynamic control of a +-configured missile is still provided by only two fins. For this reason, control effectiveness of + configuration is theoretically half of that of × configuration. Accordingly, + configuration is said to be disadvantageous when grid fins are used.

3.5 Design Space

Thickness parameter, t, is the parameter that drives mainly drag and/or axial force component. A thick-walled grid fin always creates higher drag force which is undesirable in any design condition because it is attributed as a loss for any design purpose. Therefore, under any circumstances, it is advised to choose the thinnest wall. The lower limit of this parameter is driven by the manufacturing and operating conditions. Consequently, value of t should be selected as low as manufacturing and operating conditions allow.

t/w ratio dictates the blockage area, hence the area ratio between freestream and inside of the fin cells. For subsonic to transonic flights, this parameter is related to choking phenomenon. Depending on the first critical Mach number, M_{cr1}, upper limit for t/w is fixed to a certain value to avoid choking, which causes high drag force and loss in normal force generation.

w/c ratio is an important parameter for supersonic flight regime as it is crucial in avoiding interference between flow over neighboring walls of a grid fin. Designing a non-interfering supersonic grid fin will increase the performance. For this reason, w/c ratio should be high enough so that Mach cones forming from the

walls do not interact with each other. This dictates a lower limit for w/c.

CHAPTER 4

RESULTS

In this section, a reference grid fin design on Basic Finner body [40, 41] is introduced. The design is carried out for Mach number of 0.75, which is within the transonic range.

4.1 Objective of the Sample Design

In this section, the objective of a sample design effort is explained. Design conditions and constraints are also given to identify the limits of this design campaign.

For execution of sample design, Basic Finner geometry is employed as a baseline missile. This standard geometry has been extensively used in many research studies especially in checking various test techniques and new instrumentation used in wind tunnel experiments [41]. For this reason, it is possible to find validated aerodynamic parameters of this geometry in wide range of flight conditions in numerous experimental studies. Nowadays, this geometry has been becoming more popular for validation purposes in CFD community, as well [42]. Moreover, it has been used in the investigation of novel aerodynamic devices in the literature [43]. For these reasons, aerodynamic data of Basic Finner are widely available and easily accessible, and thus, it is selected as the baseline configuration in this thesis study.

The sample design aims to create a grid fin control surface set which is operated on Basic Finner missile body and has an ability to maneuver the missile as

effective as original planar fins mounted on the same body. For this purpose, the Basic Finner geometry, illustrated in Fig. 4.1, is used as a reference model.

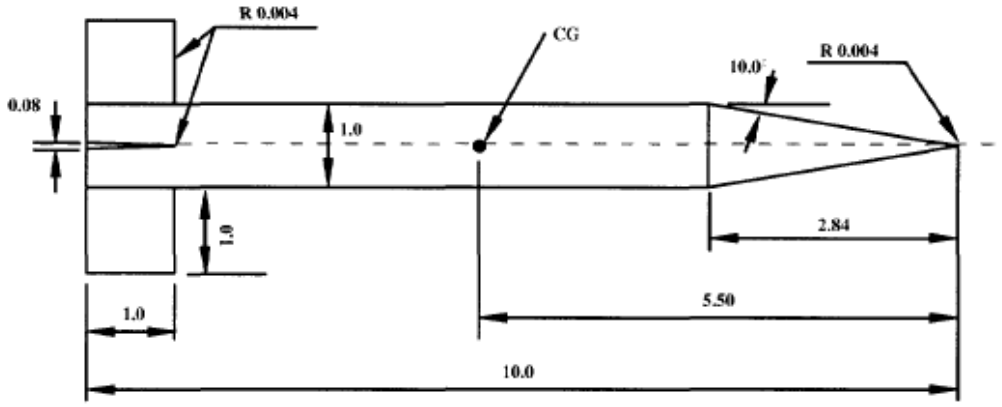

Figure 4.1: Geometric description of the Basic Finner (Dimensions are given with respect to diameter) [40]

4.1.1 Validation of Basic Finner CFD Solutions

For validation study, results of wind tunnel experiments presented by Dupuis [40] are employed. CAD model shown in Fig. 4.2, with a reference diameter of 0.4 meters, is used to conduct CFD solutions.

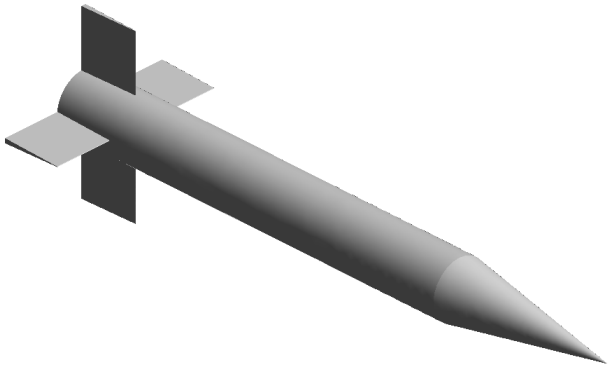

Figure 4.2: CAD model of Basic Finner used in CFD simulations

Comparison is made on the longitudinal force and moment characteristics ob-

tained by CFD runs and the experiment. These include normal force coefficient, CN, and pitching moment coefficient, Cm. As the behavior of these parameters is linear with respect to angle of attack, slopes of them definitely identify the characteristics. For this reason, normal force slope, CN_α, and pitching moment slope, Cm_α, are those that are compared.

CN_α and Cm_α data are available in the experimental data for wide range of Mach numbers. CFD solutions are conducted within a similar range. Angle of attack values used in the computations are $\alpha_1 = 0°$ and $\alpha_2 = 5°$, which are believed to be within the linear behavior range. Normal force and pitching moment slopes are calculated for each Mach number by the following numerical differentiation formulas:

$$CN_\alpha = \frac{CN_{@\alpha_2} - CN_{@\alpha_1}}{\alpha_2 - \alpha_1} \tag{4.1a}$$

$$Cm_\alpha = \frac{Cm_{@\alpha_2} - Cm_{@\alpha_1}}{\alpha_2 - \alpha_1} \tag{4.1b}$$

In Fig. 4.3, it is seen that CFD solutions and wind tunnel measurements agree well throughout the Mach range.

4.1.2 Calculation of Stability and Control Parameters of Basic Finner

Design Mach number is determined as 0.75, at which transonic phenomena mentioned in the literature (see Section 1.3), such as high drag and partial loss of control, are observed. This is accepted as a challenging design condition for grid fins, considering the transonic bucket.

In order to have a similar maneuverability, $\frac{\alpha}{\delta e}$ of the Basic Finner is taken as the objective parameter. At this point, pitch control effectiveness, $\frac{\alpha}{\delta e}$, of the reference model is calculated using CFD. Before that, CFD simulations should be validated by comparing the results to experimental data in literature.

The stability and control parameters of Basic Finner is determined via CFD solutions. Corresponding expressions for these parameters are pitching moment

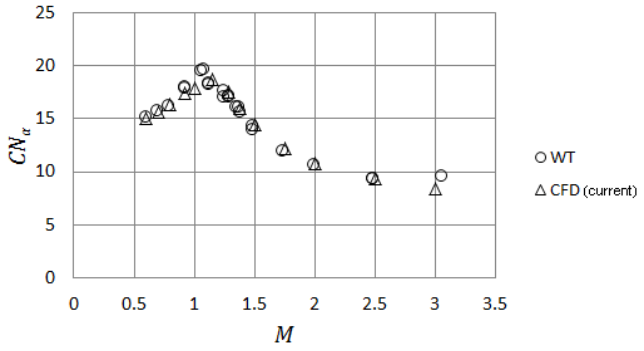

(a) Normal force slope

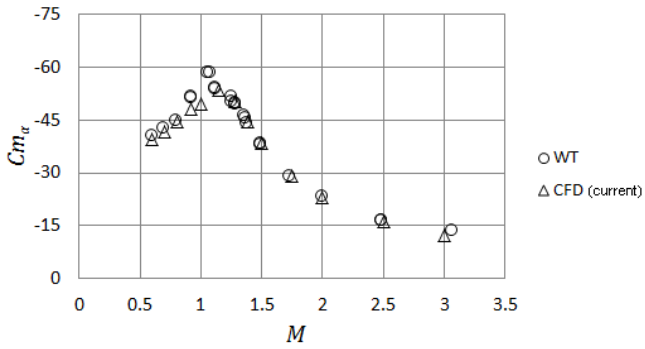

(b) Pitching moment slope

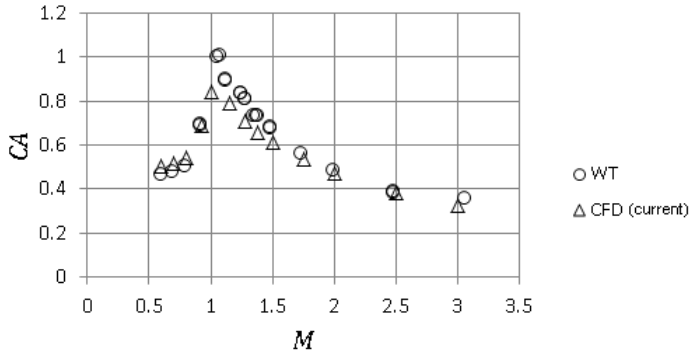

(c) Axial force

Figure 4.3: Comparison of current CFD solutions and wind tunnel experiments of Dupuis

slope, Cm_α, and pitch control effectiveness, $Cm_{\delta e}$, respectively. For determination of Cm_α, computations are conducted at two different angle of attack values; similarly, solutions at two different fin deflection angles are required to calculate $Cm_{\delta e}$. Thus, three solution configurations, which can be seen in Fig. 4.4, are utilized to calculate Cm_α and $Cm_{\delta e}$. All computations are carried out at the design Mach number of $M = 0.75$. Solved CFD cases are also listed in Table 4.1.

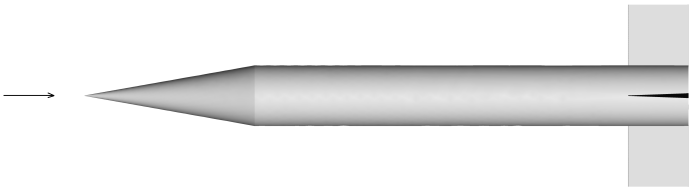

(a)

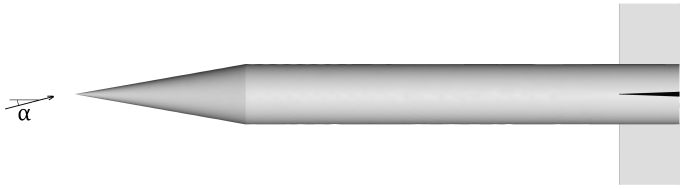

(b)

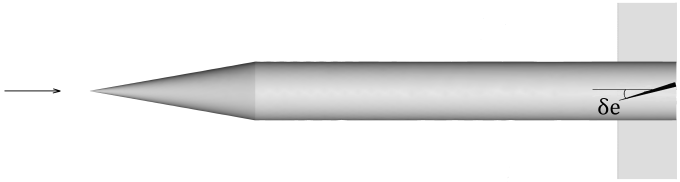

(c)

Figure 4.4: CFD models used for calculation of Cm_α and $Cm_{\delta e}$

Table 4.1: CFD cases

Case	$\boldsymbol{M}$	$\boldsymbol{\alpha}$	$\boldsymbol{\delta e}$
(a)	0.75	0°	0°
(b)	0.75	5°	0°
(c)	0.75	0°	5°

Pitching moment on center of gravity of the Basic Finner is computed in the

three cases. Following results are calculated from difference between the cases (b) and (a), and from that between cases (c) and (a), respectively: $Cm_{\alpha} = -42.4$, $Cm_{\delta e} = 34.6$. As a result, pitch control effectiveness of the Basic Finner is found as: $\frac{\alpha}{\delta e} = -0.816$

This result specifies the aim of the design effort for missile with grid fin. The objective is determined as to obtain a pitch control effectiveness of 0.816.

4.2 Employment of Unit Grid Fin Solutions

The design procedure of the grid fin set turns into an optimization of candidate geometries. To facilitate this procedure, unit grid fin (UGF) concept is introduced at the beginning of this chapter (see Section 3.2.3). In this section, how the CFD solutions of UGF are implemented into the whole problem is explained in detail.

Pitching moment is the major aerodynamic parameter in identification of fin performance. This parameter is divided into contributions from the components of the missile, which are the missile body (and all other components other than fins, if any), subscripted as 'M', and grid fin, subscripted as 'GF'. The complete missile is subscripted as 'MGF', as an abbreviation of 'missile with grid fin', while the subscript 'UGF' stands for unit grid fin. Pitching moment slope of a missile with grid fin can be expressed with Eq. 4.2, ignoring the interactions between the components. All the terms in the equation are expressed at the center of gravity location.

$$Cm_{\alpha_{MGF}} = Cm_{\alpha_M} + Cm_{\alpha_{GF}} \tag{4.2}$$

Quantity of Cm_{α_M} depends on the aerodynamic characteristics of the components other than fins. In other words, this value contains the information of the aerial vehicle on which the current grid fin design is going to be installed.

$Cm_{\alpha_{GF}}$ is the change in the pitching moment created by the grid fin at the center of gravity with respect to angle of attack. Considering a set of four grid fins each of which is composed of n UGFs, Eq. 4.3 can simply be obtained. At

this point, one can argue that the orientation of the fins ($\times$ or + configuration) matters because of the downwash and upwash effects of body. $\times$ configuration does not suffer from this issue, as it is explained in Section 3.2.2, while fins in + configuration are exposed to different effective angles of attack. However, since vertically oriented fins are affected by body in the opposite direction of horizontally oriented ones, those effects cancel out and the summation of longitudinal loads are again based on the nominal values. Therefore, Eq. 4.3 is valid independently of arrangement of fins.

$$Cm_{\alpha_{GF}} = 4 \times n \times Cm_{\alpha_{UGF}} \tag{4.3}$$

Pitch control parameter, $Cm_{\delta e}$, of a missile grid fin results from the deflection of the control surfaces, and body or any other equipment does not have a contribution at zero angle of attack. Therefore, pitch control parameter of missile with grid fin is equal to contribution of grid fin only.

When the + configuration is considered, as explained in Section 3.4, only sideward fins are active in control. Thus, only two fins are taken into account. Rotation plane of these fins are coincident with the vertical symmetry plane of the missile. Since the angle of attack is defined on the same plane as well, pitch moment derivative with respect to angle of attack can be utilized for determination of deflection characteristics of a +-configured fin set. Thus, CFD solutions at different angle of attack values will be more than enough to calculate $Cm_{\delta e_{MGF}}$ for those kind of missiles, as formulated in Eq. 4.4a.

By a similar assessment, it is argued that each fin has a potential in creating moment at the center of gravity in the case of $\times$ configuration. However, unlike the + configuration, deflection angle is not defined in the vertical symmetry plane, which causes two CFD solutions with different angle of attack values to be insufficient to characterize the aerodynamic effects of fin deflection. Hence, deflection solutions must be modeled separately defining flow angle in a proper plane. This discussion leads to Eq. 4.4b.

$$Cm_{\delta e_{MGF}} = Cm_{\delta e_{GF}} = 2 \times n \times Cm_{\alpha_{UGF}} \tag{4.4a}$$

$$Cm_{\delta e_{MGF}} = Cm_{\delta e_{GF}} = 4 \times n \times Cm_{\delta e_{UGF}} \tag{4.4b}$$

Pitch control effectiveness is calculated with the above information, by dividing Eq. 4.4 by Eq. 4.2 and inserting Eq. 4.3 into the latter. As a result, $\frac{\alpha}{\delta e}$ is expressed using the parameters to be obtained by CFD solutions of UGF models. Eqs. 4.5a and 4.5b address to + and × configurations, respectively.

$$\frac{\alpha}{\delta e} = \left(\frac{Cm_{\delta e}}{Cm_{\alpha}}\right)_{MGF} = \frac{2 \times n \times Cm_{\alpha_{UGF}}}{Cm_{\alpha_M} + 4 \times n \times Cm_{\alpha_{UGF}}} \tag{4.5a}$$

$$\frac{\alpha}{\delta e} = \left(\frac{Cm_{\delta e}}{Cm_{\alpha}}\right)_{MGF} = \frac{4 \times n \times Cm_{\delta e_{UGF}}}{Cm_{\alpha_M} + 4 \times n \times Cm_{\alpha_{UGF}}} \tag{4.5b}$$

After having derived the expressions for pitch control effectiveness, a discussion about the relation with static stability of the missile body, which is denoted by Cm_{α_M}, should be made. Magnitude and sign of this value is said to be crucial in terms of applicability of a grid fin control system because $\frac{\alpha}{\delta e}$ is strongly dependent on Cm_{α_M}. In Eq. 4.5a, in case of $Cm_{\alpha_M} = 0$, $\frac{\alpha}{\delta e}$ will take a value of 0.50, which will be lower for negative values of Cm_{α_M}. This statement is independent of the quantity of $Cm_{\alpha_{UGF}}$; hence, designing an effective grid fin for 'stable without fins' vehicles is not considered. Therefore, an 'unstable body' is required to start a grid fin design with the method presented in this thesis. A similar assessment might be done for Eq. 4.5b, by roughly presuming the following relation, which is due to orientations of angle of attack and deflection planes:

$$\frac{Cm_{\delta e_{UGF}}}{Cm_{\alpha_{UGF}}} \approx \sin 45^{\circ}$$

Using UGF models results in certain level of errors due to assumptions. Possible sources of errors and weaknesses are listed below:

1. Aerodynamic interference of grid fins with the missile body and other components is ignored. This occurrence gets significant as the planned location of fins moves towards nose of missile since more region will be affected by the wake of the grid fins.

2. External frame and connecting elements of grid fin are not taken in the account.

3. Up- and downwash effects of body are presumed to be in balance such that total loads of four grid fins does not deviate from nominal.

4.2.1 Description of CFD solution cases

Calculation of $Cm_{\alpha_{UGF}}$ and $Cm_{\delta e_{UGF}}$ quantities requires CFD solutions of a UGF model, previously represented in Fig. 3.14, at two different flow angle arrangements. As done in validation campaign of Basic Finner (see Section 4.1.2), in addition to 0° angle of attack and deflection case, solutions are needed at a non-zero angle of attack and deflected cases for the calculation of $Cm_{\alpha_{UGF}}$ and $Cm_{\delta e_{UGF}}$, respectively. Angular quantities are assumed to be within the linear behavior range of grid fin.

Walls of a grid fin set arranged in + configuration lie in diagonal directions (see Fig. 4.5a), while they lie in principal directions in case of × configuration (see Fig. 4.5b). In this thesis study, × configuration is selected as a result of the assessment in Section 3.4. For this reason, orientation of UGF in CFD simulations are arranged in principal directions.

Flow direction is defined using the coordinate axes shown in Fig. 4.5. By right hand rule, x-axis can be inferred as in the direction of nose of the missile, or leading edge of the grid fin. By definition, angle of attack is given in the zx-plane. Therefore, unit vector of the freestream velocity is expressed as $[-\cos(\alpha)\hat{i} - \sin(\alpha)\hat{k}]$, considering sign conventions.

$Cm_{\delta e}$ appears in Eq. 4.5b and it is calculated for only × configured fin set. For this configuration, deflection axes of grid fins are parallel to 45° and −45° lines in yz-plane. Therefore, in order to simulate the flow over a deflected fin, the velocity vector relative to coordinate system fixed to UGF should be defined. This vector is obtained by rotating the vector expression determined for + configuration about x-axis by negative 45°. Thus, following rotation matrix multiplication is done to express the same vector in the frame of fin #1, which is the upper-right one looking from the rear:

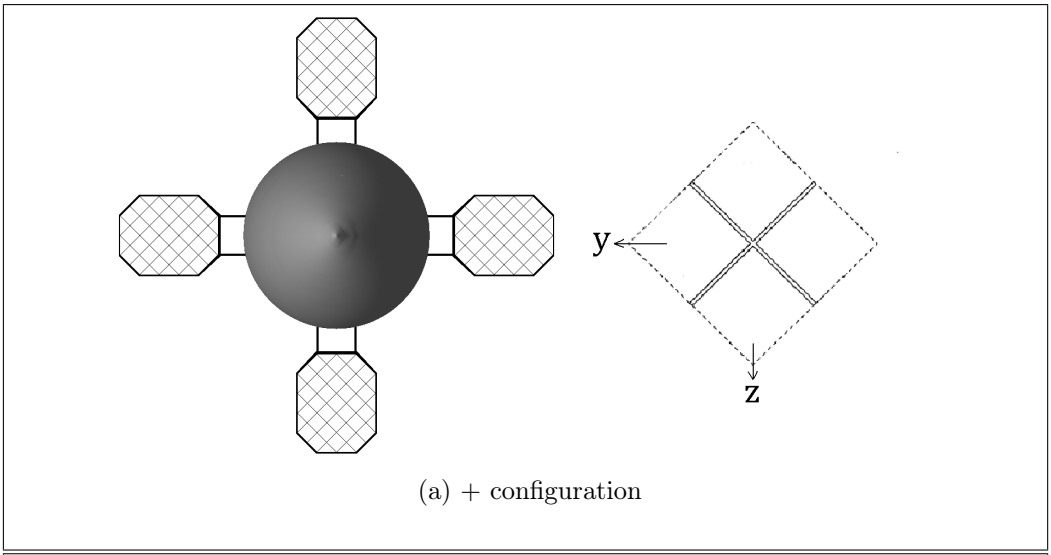

(a) + configuration

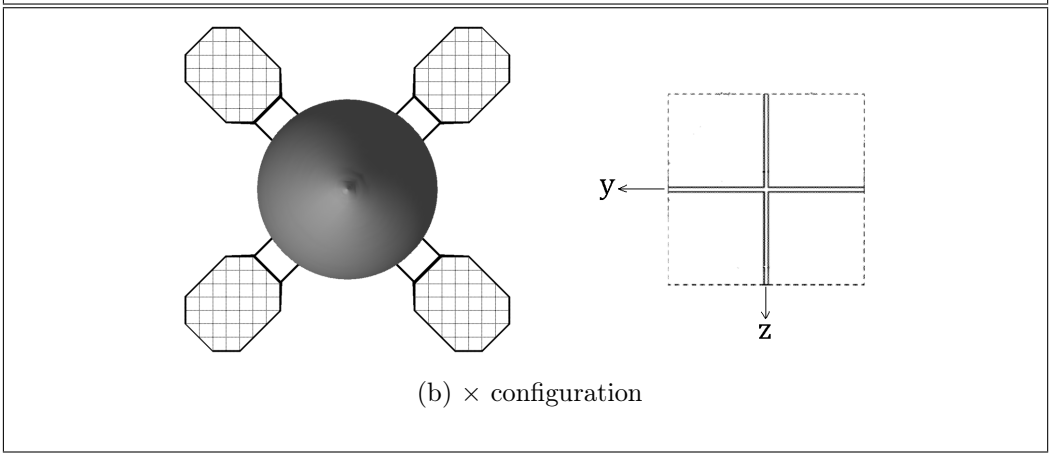

(b) × configuration

Figure 4.5: Matching configurations of MGF and UGF (forward view)

$$\begin{bmatrix} 1 & 0 & 0 \\ 0 & \cos(-45^\circ) & -\sin(-45^\circ) \\ 0 & \sin(-45^\circ) & \cos(-45^\circ) \end{bmatrix} \begin{Bmatrix} -\cos\delta e \\ 0 \\ \sin\delta e \end{Bmatrix}$$

When multiplication is done, unit vector of relative velocity, which is to be assigned to the pressure-far-field type of boundaries, is found as

$$\left[-\cos(\delta e)\hat{i} + \frac{\sin(\delta e)}{\sqrt{2}}\hat{j} + \frac{\sin(\delta e)}{\sqrt{2}}\hat{k} \right].$$

For other fins, sign of the $\hat{j}$ term can be either $-$ or $+$. Because lateral force and moment components are out of interest, this unit vector representation is valid for all fins.

4.3 Design Space of the Sample Design

Current design effort is made to arrange an optimum grid fin control set for a 0.4 m diameter Basic Finner body at design Mach number 0.75, as stated before. In order to specify the design space, the geometric parameters are investigated one-by-one. t/w, w/c and c/D are the dimensionless parameters introduced in the previous chapter.

Thickness of the walls, t, is determined based on the discussion in Section 3.5. As the value of t is arranged as small as manufacturing conditions allow, a unique value is assigned for this parameter. Amount of this value does not influence the remaining of the design process, so $t = 1$ mm is assigned as a 'safe' value.

Upper limit of t/w is determined considering choking phenomenon that is avoided by utilizing area rule for $M = 0.75$. Corresponding critical area ratio for $M = 0.75$ is calculated by Eq. 2.3 as 0.9412. Ratio of outflow to inflow cross-sectional areas in a generic grid fin cell is

$$\frac{(w-t)^2}{w^2} = 0.9412 \longrightarrow \frac{w-t}{w} = 0.9702$$

therefore, critical thickness-over-width ratio,

$$\left(\frac{t}{w}\right)_{cr} = 0.0298,$$

is the upper limit in the design space to avoid choking.

Chord parameter, c, is desired to be maximum to increase the lifting surface area. For this reason, c is also assigned a unique value, like done for t. Limit for the maximum chord value is set by the geometric constraints. For example, a tube-like launcher station for missile is a candidate for constituting geometric constraint, in case fins are stowed on the missile body and placed in the tube in that way. Total length of 2 chords and missile diameter should not exceed the launcher diameter. Consequently, chord parameter is selected as 10% of the diameter. In other words, c/D is assigned to 0.1.

The parameter w/c is limited by 10 in order to prevent extremely and unrealistically high width values.

Design space is constructed decreasing t/w from maximum value by a step size of 0.0025, as seen in Table 4.2. 12^{th} design point has such a large width value that is equal to diameter of missile. Hence, proceeding beyond this design point would yield an impractical solution. After solutions are obtained, it is decided to add two more points between design points 11 and 12, for refinement purpose. Values of parameters and full set of design points are listed in Table 4.2.

Table 4.2: Design points (Dimensional parameters are given in milimeters.)

D	c/D	c	t
400.0	0.1	40.0	1.0

#	t/w	w	w/c	**Remarks**
1	0.03000	33.3	0.833	Maximum t/w
2	0.02750	36.4	0.909	
3	0.02500	40.0	1.000	
4	0.02250	44.4	1.111	
5	0.02000	50.0	1.250	
6	0.01750	57.1	1.429	
7	0.01500	66.7	1.667	
8	0.01250	80.0	2.000	
9	0.01000	100.0	2.500	
10	0.00750	133.3	3.333	
11	0.00500	200.0	5.000	
12	0.00250	400.0	10.000	Extreme width
13	0.00375	266.7	6.667	Refinement point 1
14	0.00300	333.3	8.333	Refinement point 2

4.4 Calculations at Design Points

CFD solutions are conducted for UGF model in $\times$ configuration at design points given in Table 4.2. For domain and mesh creation, the same methodology is performed as in Section 3.2.3. Three solutions per design point are carried out, as shown in Table 4.3. The rightmost column contains unit vector representations of direction of freestream velocity.

Table 4.3: CFD cases solved at each design point

Case	$\boldsymbol{M}$	$\boldsymbol{\alpha}$	$\boldsymbol{\delta e}$	$\frac{\vec{\boldsymbol{V}}}{\lvert\vec{\boldsymbol{V}}\rvert}$
(a)	0.75	0°	0°	$[\ -1.0000 \quad 0.0000 \quad 0.0000\ ]^T$
(b)	0.75	5°	0°	$[\ -0.9962 \quad 0.0000 \quad -0.0872\ ]^T$
(c)	0.75	0°	5°	$[\ -0.9662 \quad 0.0616 \quad 0.0616\ ]^T$

Purpose of obtaining the results of these cases is to acquire the necessary quantities and to determine n in the Eq. 4.5b for each design point. Then, the optimum design point, which yields minimum drag force, is to be determined.

If Equation 4.5b is solved for n, following relation is obtained

$$n = \frac{\frac{\alpha}{\delta e} \times Cm_{\alpha_M}}{4 \times Cm_{\delta e_{UGF}} - 4 \times \frac{\alpha}{\delta e} \times Cm_{\alpha_{UGF}}} \tag{4.6}$$

where Cm_{α_M} is calculated by solving body geometry alone and it has a value of 4.98. This means that it is possible to find a sufficient number of UGFs that satisfies a certain amount of pitch control effectiveness, which is previously determined as an objective of the sample design.

To calculate the pitching moment created by UGF at center of gravity of the missile as required by 4.6, normal force on the UGF, which is defined in missile coordinate axes, is obtained as the output of CFD solution. Pitching moment is calculated through Eq. 4.7

$$Cm_{UGF} = CN_{UGF}\frac{l_{GF}}{l_{ref}} \tag{4.7}$$

where l_{GF} denotes the moment arm of grid fin, as shown in Fig. 4.6 and reference length, l_{ref} is equal to the diameter of body, which is 0.4 m.

Equation 4.7 enables writing following two relations:

$$Cm_{\alpha_{UGF}} = CN_{\alpha_{UGF}}\frac{l_{GF}}{l_{ref}} \tag{4.8}$$

$$Cm_{\delta e_{UGF}} = CN_{\delta e_{UGF}}\frac{l_{GF}}{l_{ref}} \tag{4.9}$$

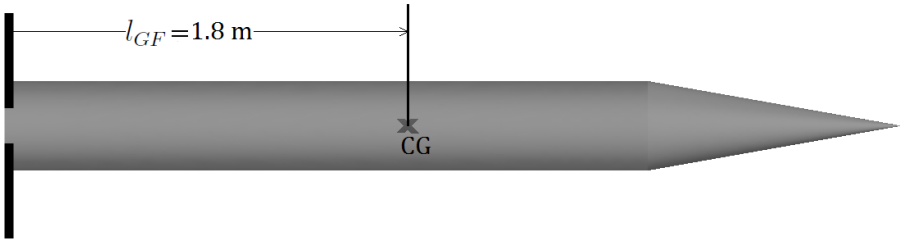

Figure 4.6: Moment arm of the GF set

Normal force derivatives, CN_α and $CN_{\delta e}$, are calculated by numerical differentiation:

$$CN_{\alpha_{UGF}} = \frac{CN_{UGF_{@(b)}} - \cancelto{0}{CN_{UGF_{@(a)}}}}{\alpha_{@(b)} - \cancelto{0}{\alpha_{@(a)}}} \tag{4.10}$$

$$CN_{\delta e_{UGF}} = \frac{CN_{UGF_{@(c)}} - \cancelto{0}{CN_{UGF_{@(a)}}}}{\delta e_{@(c)} - \cancelto{0}{\delta e_{@(a)}}} \tag{4.11}$$

As a result, required number of UGFs providing $\frac{\alpha}{\delta e} = -0.816$ is calculated for each design point and listed in Table 4.4.

Table 4.4: Required n values for design points

#	t/w	w	w/c	n
1	0.03000	33.3	0.833	109
2	0.02750	36.4	0.909	138
3	0.02500	40.0	1.000	75
4	0.02250	44.4	1.111	56
5	0.02000	50.0	1.250	42
6	0.01750	57.1	1.429	31
7	0.01500	66.7	1.667	22
8	0.01250	80.0	2.000	15
9	0.01000	100.0	2.500	7
10	0.00750	133.3	3.333	6
11	0.00500	200.0	5.000	4
12	0.00250	400.0	10.000	5
13	0.00375	266.7	6.667	4
14	0.00300	333.3	8.333	3

It should be remembered that, by employment of required number of UGFs, all

design points have the same $\frac{\alpha}{\delta e}$, which is 0.816. However, they vary in being an efficient design, which means the drag force created by each design selection has a different value. CFD solutions of case (a) (see Table 4.3) are utilized in order to calculate drag contributions of design choices. This is done by Eq. 4.12

$$CD_{GF} = n \times CD_{UGF} \tag{4.12}$$

Variation of drag force on the design alternatives is plotted in Figure 4.7. It is seen that there exists a minimum drag force between DP9 and DP11. These are accounted as candidates for the most efficient, i.e., optimum design. Note that these are the values corresponding to internal faces that are represented by unit grid fin.

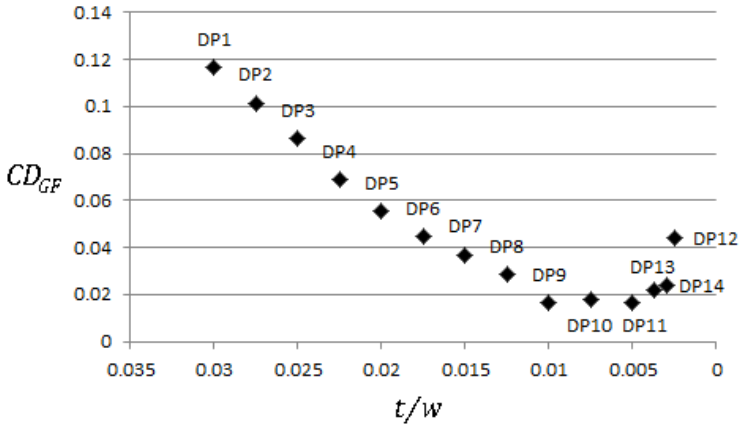

Figure 4.7: Drag coefficients of design alternatives

A new parameter, characteristic length, L, is defined to have a sense for overall dimensions of the grid fin. This has a theoretical definition considering that UGFs are placed in a square-shaped frame. Such a definition allows comparing the possible dimensions of a grid fin in use of each design alternative.

$$L = w \times \sqrt{n} \tag{4.13}$$

Variation of characteristic length is plotted in Fig. 4.8. DP9 is observed as the most advantageous alternative in the aspect of overall dimension. As a consequence of evaluation of design alternatives, DP9 is selected as the optimum solution, which, according to Table 4.4, has $n = 7$ UGFs.

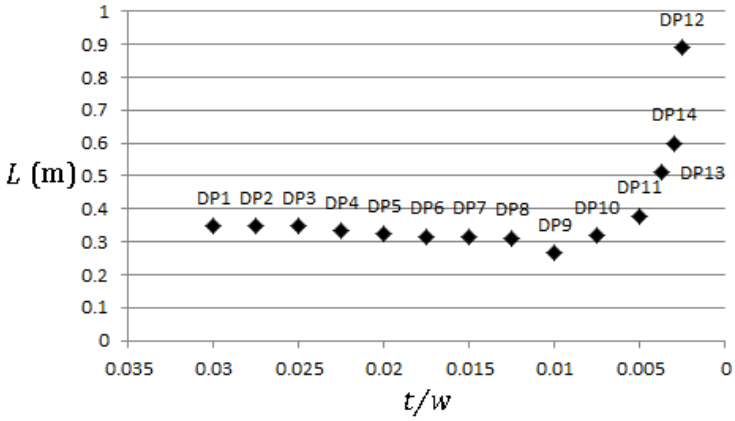

Figure 4.8: Characteristic lengths of design alternatives

4.5 The Full MGF Model of Optimum Solution

The grid fin resulted from the optimization procedure is created as a CAD model. As calculated in previous section, number of repetitions, n, is aimed to have a value approximately equal to 7. Pattern of UGFs and symmetry issues result in the geometry shown in Fig. 4.9a with $n = 8$. This GF has 5 of type 1, 4 of type 2 and 4 of type 3 nodes.

Optimized grid fin is mounted on body of Basic Finner and CFD solutions are conducted on this geometry. Thus, control, stability and drag quantities estimated by UGF model are compared with those calculated for MGF model. Front view of CAD model of MGF is seen in Figure 4.9b.

4.5.1 Mesh Independence Study

The mesh independence study is conducted on three meshes having coarse, medium and fine intensities.

Three different meshes are created by changing growth rates of both triangular surface elements and tetrahedral volume elements. The surface meshes on the missile with grid fin geometry are created by means of ANSYS 14.0, while TGrid 5.0 is used in creation of 3-D elements. The surface meshes created for this study are shown in Figures 4.10 and 4.11. Boundary layers are resolved by prismatic

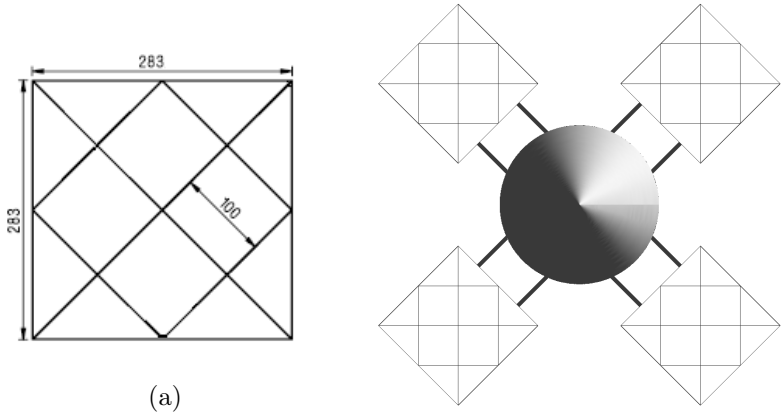

(a) (b)

Figure 4.9: Optimum GF and MGF geometries

cells grown from the triangular surface elements. The thickness of the first prism layer is fixed to assure that the y^+ value is maintained around the order of 1. The aspect ratio of elements in the last layer is kept as 4 throughout all the wall boundaries, in order to have smooth transitions between neighboring elements. 10 prism layers are created for each triangular boundary face.

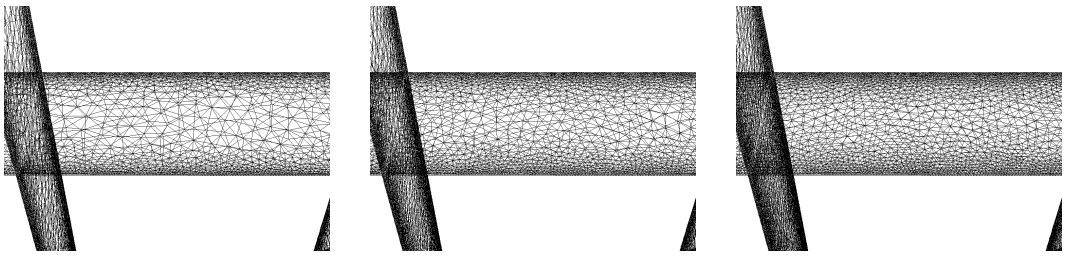

(a) Coarse (b) Medium (c) Fine

Figure 4.10: Surface meshes on the grid fin surfaces

ANSYS FLUENT 14.0 solver is utilized to run the simulations with the same settings as those employed in validation runs in the previous chapter. $M_\infty = 0.75$ is assigned as the freestream conditions. Freestream pressure and temperature values are taken from ISA table at sea-level conditions. Aerodynamic force and moment values at the wall boundaries are computed after satisfactory convergences are achieved. Force quantities are nondimensionalized using freestream dynamic pressure and reference area, S_{ref}, while moment coefficients are ob-

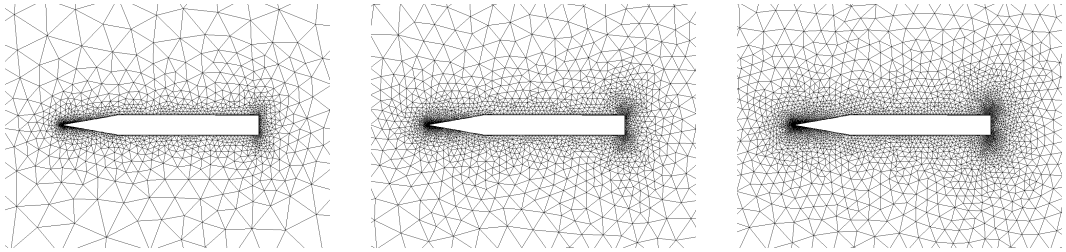

(a) Coarse (b) Medium (c) Fine

Figure 4.11: Volume meshes in vertical symmetry plane

tained using the reference length, l_{ref}, in addition to other two. Reference area and length values are determined as cross-sectional area and diameter of missile body, respectively, which are 0.1257 m^2 and 0.4 m.

The parameters investigated in the independence study are axial force coefficient, CA, normal force coefficient, CN, and pitching moment coefficient, Cm, acted on missile with grid fin surface. CA is calculated for zero angle of attack in order to determine the accuracy of drag prediction. CN and Cm are computed using the solutions at $\alpha = 4°$. The difference between the simulations with medium and fine mesh is around 1% for each parameter (see Table 4.5). Therefore, it is concluded that medium mesh provides satisfactory mesh resolution.

Table 4.5: Axial and normal force results with different meshes

	Number of elements	$\boldsymbol{CA}$	**Rel. error**	$\boldsymbol{CN}$	**Rel. error**	$\boldsymbol{Cm}$	**Rel. error**
Coarse	6,024,060	0.652	-	0.902	-	−2.622	-
Medium	8,319,076	0.626	4.15%	0.870	3.68%	−2.544	3.06%
Fine	11,684,950	0.620	0.96%	0.860	1.16%	−2.520	0.95%

4.5.2 CFD Solutions of MGF Model

In this section, results of CFD analyses conducted on MGF model are presented and they are compared to the parameters obtained by the UGF model. CFD solutions of MGF model are carried out at conditions listed in Table 4.6. $Cm_{\alpha_{MGF}}$, $Cm_{\delta e_{MGF}}$, $\dfrac{\alpha}{\delta e}$ and CD_{fin} parameters are calculated in the same method as in

Eq. 4.1.

Table 4.6: CFD cases

Case	$\boldsymbol{M}$	$\boldsymbol{\alpha}$	$\boldsymbol{\delta e}$
(a)	0.75	0°	0°
(b)	0.75	5°	0°
(c)	0.75	0°	5°

Comparison is made between the results obtained in Section 4.3 and MGF solutions. Loads on exterior frame and connecting rods of grid fins are excluded from the comparison for consistency. However, 'frame & rods included' results are also presented to show the contribution of these components. Also, the same parameters of Basic Finner are listed in Table 4.7.

Table 4.7: Comparison of resulting parameters

	calc. by UGF ($n = 7$)	**calc. by MGF (frame & rods excld.)** ($n = 8$)	**calc. by MGF (frame & rods incld.)** ($n = 8$)	**BF (planar fins)**
$\boldsymbol{Cm_{\alpha}}$	-14.1	-19.2	-35.3	-42.4
$\boldsymbol{Cm_{\delta e}}$	11.5	16.2	28.9	34.6
$\boldsymbol{\alpha/\delta e}$	-0.815	-0.844	-0.818	-0.815
$\boldsymbol{CD_{fin}}$	0.0165	0.0204	0.0565	0.0599

The results show that Cm_{α} and $Cm_{\delta e}$ are underestimated by utilization of UGF. Large part of the error margin is originated from different values of number n. As mentioned before, although n is calculated as 7 for DP9, the fin can be modeled in a pattern such that $n = 8$. This fact increases both parameters in the full model solution. However, ratio of $Cm_{\delta e}$ readings in 1$^{\text{st}}$ and 2$^{\text{nd}}$ columns of Table 4.7 is less than $\frac{7}{8}$. This difference can be concluded as error arising from UGF model. This type of error can be associated with the number of UGFs, n, since when it has a smaller value, validity level of the representation of UGFs decreases. In order to explain this statement, two different grid fin examples, which are shown in the previous sections of the thesis, are presented here again. The one in the Fig. 4.12a involves much more nodes, thus, much more the internal "type 1" nodes, which are fully represented by the UGF model. On

the contrary, within the fin in Fig. 4.12b, there is no dominance of "type 1" nodes and number of the other types of nodes is also significant. Owing to large number of these 'less-representative' nodes, modeling error might increase and this might negatively affect the success of the UGF model. The deviation in Cm_α and $Cm_{\delta e}$ readings between 2$^{\text{nd}}$ and 3$^{\text{rd}}$ columns is also associated with the same situation, as the importance of contributions of frame & rods is much higher with decreasing n. Fortunately, these two parameters are calculated relatively close to those of Basic Finner in this particular problem when loads on frame & rod components are taken into account.

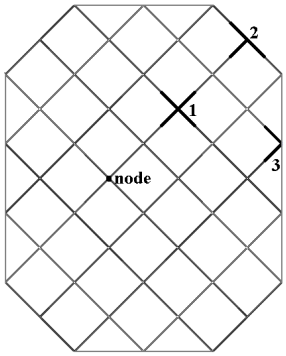

(a) A high n grid fin ($n = 38$)

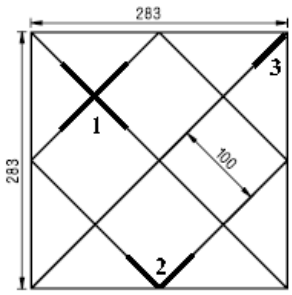

(b) A low n grid fin ($n = 8$)

Figure 4.12: Two grid fin examples

In spite of the deviation in parameters Cm_α and $Cm_{\delta e}$ between UGF and MGF solutions, $\frac{\alpha}{\delta e}$ values calculated by any of the methods agree well, as well as they agree with data of Basic Finner. Compared to planar fins, less value of drag force obtained with use of grid fins, even when frame and connecting rods are included in the calculation. Nevertheless, the frame geometry, i.e. thickness, might be unrealistic since the structural concerns are not taken into consideration, therefore, it is not easy to claim that the current grid fin design is more efficient than the planar fins of the Basic Finner in terms of drag characteristics. The frame and rod thicknesses are used as 1 mm and 10 mm, respectively, in this study.

Total drag on all four fins is of the same order of magnitude as the drag on body component, which has a value of 0.286. Therefore, minimization of the fin drag

is concluded as an important issue for overall performance.

Dimensional comparison of the current grid fin design and the planar fin set of Basic Finner is shown in Fig. 4.13. Grid fins occupy less volume compared to planar fins, although their effectivenesses are almost equivalent. In addition, dimensions of the current grid fin allows stowing the fins on the missile body. Each grid fin should fit on a quarter of circumference of the body cross-section, when they are stowed, in order to have a superior packaging feature, which is introduced as one of the motivation issues for designing a grid fin. Quarter circumference is calculated as $\frac{1}{4}\pi D = 314$ mm, while total width of one grid fin is 288 mm. The sketch of this scenario is shown in the Fig. 4.14, which shows that stowed fins are not encountered by any mechanical engagement with each other. The stowing issue is further improved by the study conducted in Section 4.6.

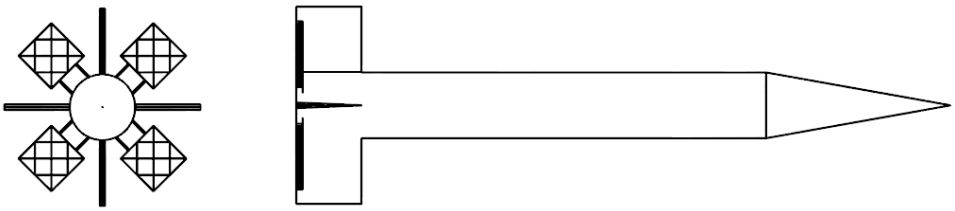

Figure 4.13: Dimensions of planar and current grid fins on Basic Finner body

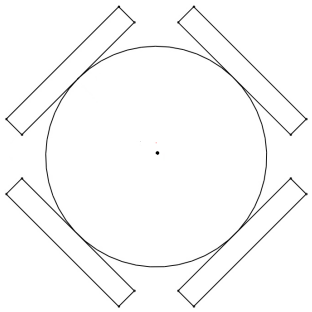

Figure 4.14: Sketch of the stowing scenario

4.5.3 Hinge Moment Characteristics of Current Grid Fin Design

Hinge moment characteristics of current grid fin design is studied in comparison with baseline planar fin model. Hinge moment requirement to operate grid fin is anticipated lower than that required for planar fin, because of minimal change in center of pressure location of grid fin in chordwise direction. To conduct a proper comparison, CFD solution are carried out for MGF and BF configurations. This is done within an angle of attack range in order to be able to create a displacement in center of pressure. After the solutions are run, aerodynamic moments about the hinge lines of both components are obtained.

Hinge lines of grid fins are usually coincident with the centerline (see Fig. 4.15). However, for planar fins, there is no common hinge axis defined. As a usual practice, a hinge axis yielding the minimum hinge moment requirement is determined, by considering all flight conditions that the missile is going to be exposed. That is, determination of hinge axis takes place after the solution data are obtained. For this purpose, in this study, aerodynamic moment and force data are acquired at an arbitrary point, which is the trailing edge of the fin, and they are moved freely to an intended location. In this study, flight conditions are determined as:

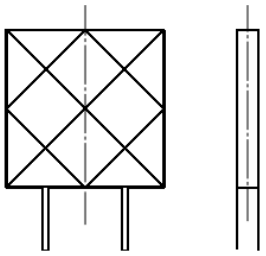

Figure 4.15: Hinge line of grid fin

$$M = 0.75 \ \& \ \alpha = \{0°, 2°, 4°, 6°, 8°, 10°, 12°, 15°\}$$

At these conditions, CFD simulations are conducted for both fins and aerodynamic force and moment exerted on each fin are computed. Force and moments are expressed in coefficient form, which is obtained using reference area,

$S_{ref} = 0.1257$ m^2, and reference length, $l_{ref} = 0.4$ m, which are equal to cross-sectional area and diameter of the missile body, respectively. Hinge moment coefficients of grid fin in different flow conditions are listed in Table 4.8.

Table 4.8: Hinge moment coefficient data of the grid fin

$\boldsymbol{\alpha}$	$\boldsymbol{Cm_{h_{GF}}}$
0°	0.00×10^{0}
2°	1.58×10^{-3}
4°	2.61×10^{-3}
6°	2.23×10^{-3}
8°	3.72×10^{-3}
10°	4.21×10^{-3}
12°	4.54×10^{-3}
15°	4.77×10^{-3}

For planar finned Basic Finner, aerodynamic normal force and moment coefficients calculated at the trailing edge are listed in Table 4.9. The values are used to calculate the hinge moment values at each angle of attack. The hinge moment data of planar fin can be carried to any longitudinal position applying Eq. 4.14. At a certain location, maximum of hinge moments in all angle of attack conditions has the minimum value, as seen in Fig. 4.16.

Table 4.9: Normal force and moment data of planar fin expressed at the trailing edge

$\boldsymbol{\alpha}$	$\boldsymbol{CN_{fin}}$	$\boldsymbol{Cm_{te}}$
0°	0.00×10^{0}	0.00×10^{0}
2°	1.76×10^{-1}	1.36×10^{-1}
4°	3.64×10^{-1}	2.77×10^{-1}
6°	5.79×10^{-1}	4.17×10^{-1}
8°	7.37×10^{-1}	5.32×10^{-1}
10°	9.60×10^{-1}	6.22×10^{-1}
12°	1.04×10^{0}	6.49×10^{-1}
15°	1.16×10^{0}	6.90×10^{-1}

$$Cm_{h_{PF}} = Cm_{te} - \frac{x - x_{te}}{l_{ref}} CN_{fin} \tag{4.14}$$

where subscript te stands for "trailing edge" and x is the coordinate in missile axial direction.

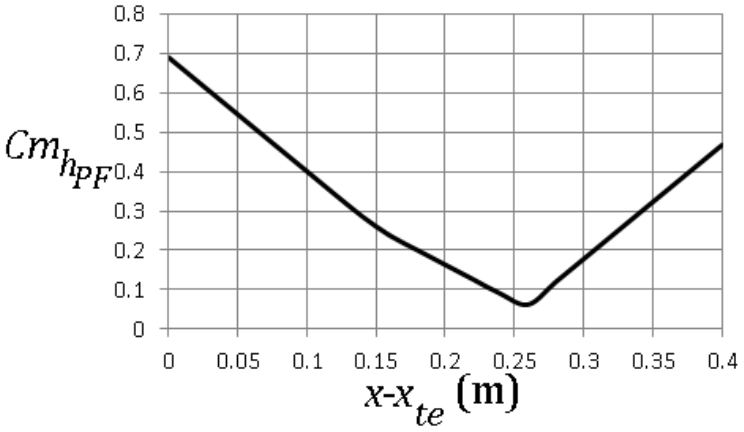

Figure 4.16: Maximum hinge moment vs. hinge location on planar fin

The distance between the most efficient hinge location and the trailing edge is calculated as 0.258 meters. Table 4.10 shows the hinge moment coefficients with respect to angle of attack at the most efficient hinge location. It also includes the hinge moment data of the grid fin (shown in Table 4.8) for comparison purpose.

Table 4.10: Hinge moment comparison of planar fins of Basic Finner and current grid fin design

α	$Cm_{h_{PF}}$	$Cm_{h_{GF}}$
0°	0.00×10^{0}	0.00×10^{0}
2°	2.24×10^{-2}	1.58×10^{-3}
4°	4.16×10^{-2}	2.61×10^{-3}
6°	4.32×10^{-2}	3.23×10^{-3}
8°	5.65×10^{-2}	3.72×10^{-3}
10°	2.50×10^{-3}	4.21×10^{-3}
12°	1.92×10^{-2}	4.54×10^{-3}
15°	5.65×10^{-2}	4.77×10^{-3}
Max.	5.65×10^{-2}	4.77×10^{-3}

As seen in Table 4.10, hinge moment of the planar fin is about ten times higher than that of grid fin, even when the hinge location of the planar fin is selected as the most efficient. This is a result of large amount of displacement of center of pressure on the planar fin. Power requirement of actuation motors is reduced when currently designed grid fin is used.

4.6 Curved Grid Fin

In this section, a drag reduction technique is applied to the present grid fin design. This grid fin has equivalent flight control characteristics with given conventional planar fin, and it is aimed to obtain a further improvement in its efficiency and design on drag and packaging characteristics.

A couple of drag reduction techniques is mentioned under the literature survey (see Section 1.3). Two most popular examples are sweptback grid fins and grid fins with sharp leading edges [8, 26, 27]. Both methods are based on weakening the high pressure region formed after stagnated flow in front of the leading edges. Utilizing each method alone or both together, instead of a strong pressure wave, a number of weaker waves is obtained, as schematically represented in Fig. 4.17.

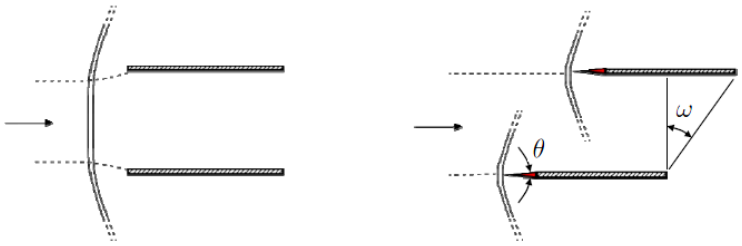

Figure 4.17: Weakening the stagnation regions by leading edge sharpness and backsweep angles [26]

A similar approach is proposed by Li *et al.*, who introduced "circular-arc grid fins" in order to reduce drag force in low supersonic speeds [29]. Circular-arc (or curved) grid fins also create an offset between the leading edges of the grid fin. Therefore, a drag reduction is expected in transonic flow, too, as a similar effect with sweptback grid fins. Moreover, curved grid fins provide a further convenience in stowing the fins on the missile body, if they are designed in such a way that the leading edges match the missile body surface when they are stowed (see Fig. 4.18). This necessitates that the radius of curvature of grid fin is equal to radius of the missile body. After these assessments, the curved grid fin analyzed in the current study is determined as shown in Fig. 4.19b. Flat grid fin model, which is developed in the previous section, is shown in Fig. 4.19a.

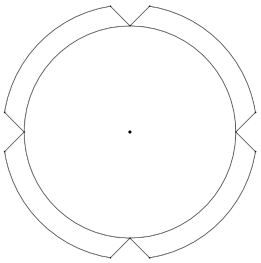

Figure 4.18: Sketch of stowing scenario of curved grid fin

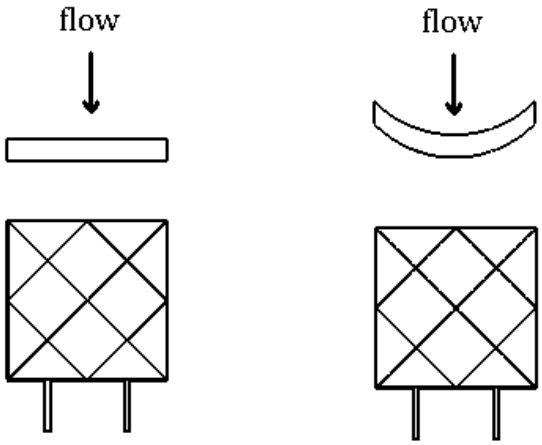

(a) Flat grid fin model (b) Curved grid fin model

Figure 4.19: Grid fin models in the transonic drag reduction study

4.6.1 Comparison of the Results of Missiles with Flat and Curved Grid Fins

The mesh on the curved grid fin is generated with the same parameters (growth rate, *etc.*) as medium mesh of flat grid fin, in order to ensure obtaining a proper comparison between two models.

The effects of curved grid fin application on missile body are examined by a number of simulations at design Mach number, $M = 0.75$, and sea-level standard conditions. The simulations are conducted at varying angle of attack values, the range of which is $[0°, 15°]$. Investigation of aerodynamic behavior of the two models are made in aspects of overall aerodynamic properties of missile with grid fins and hinge moment characteristics of the grid fins.

Use of curved grid fins results in a decrease in drag force on the whole missile, as shown in Fig. 4.20c. This reduction has a magnitude up to 4% relative to drag force on missile with flat grid fins. The difference in drag created by the two models decreases as angle of attack is being raised. No significant change in normal force on the missile is observed in use of the two different grid fins as seen in Fig. 4.20a. It is observed that pitching moment values are slightly lower in the case of curved grid fin application. The reason for this is that the center of pressure of curved grid fins is located at more forward relative to that of flat ones.

Hinge moment characteristics is the second issue that is studied for the curved grid fin. The CFD simulations that is used for determination of overall aerodynamic properties are again utilized in order to determine the aerodynamic moment exerted on a single grid fin about its hinge axis. In this particular study, only the grid fin surfaces (including the frame and connecting rods) are acquired as the output of FLUENT solver.

Hinge axes of grid fin models are defined as the geometric centerline of connecting rods. Sketch of the centerlines is presented in Fig. 4.21. The hinge axis of curved grid fin is located at 15 mm forward of hinge line of the flat grid fin.

Hinge moment data taken from the CFD simulations are presented in Table 4.11 and Fig. 4.22. The results show that application of curved grid fins increases the actuator requirement with a great significance. It is also remarkable that the maximum hinge moment on curved grid fin is approximately half of the value calculated for the planar fin in Section 4.5.3. Furthermore, it is possible to improve hinge characteristics of curved grid fin by selection of a better hinge axis, which is located as close as possible to the center of pressure of fins, with an appropriate mechanical design.

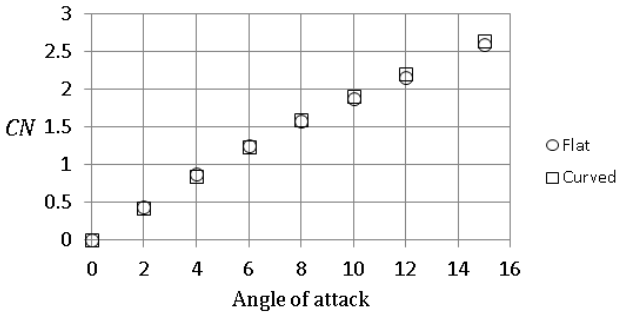

(a) Normal force coefficient

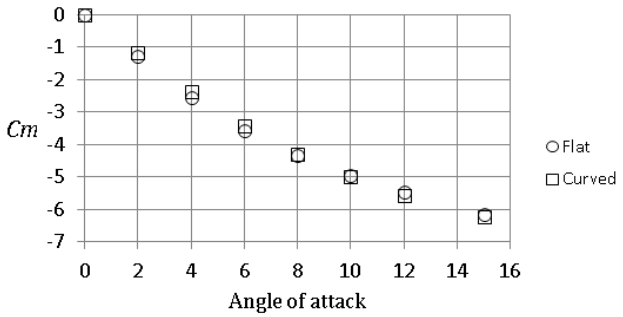

(b) Pitching moment coefficient

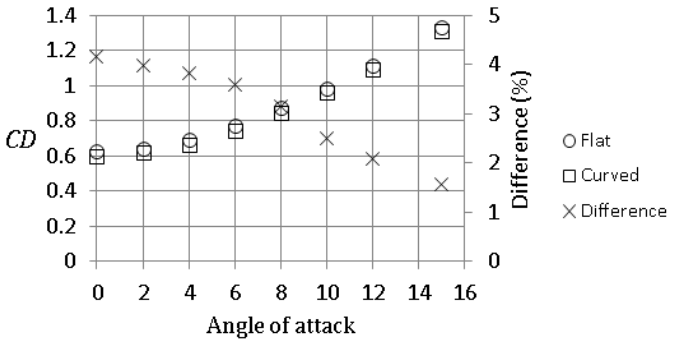

(c) Drag coefficient

Figure 4.20: Aerodynamic force and moment comparison of the two models

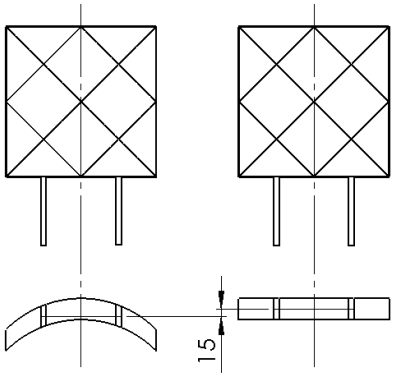

Figure 4.21: Hinge lines of the curved and the flat grid fin models

Table 4.11: Hinge moment comparison of planar fin and current grid fin designs

$\boldsymbol{\alpha}$	$\boldsymbol{Cm_{h_{PF}}}$	$\boldsymbol{Cm_{h_{GF}}}$ (flat)	$\boldsymbol{Cm_{h_{GF}}}$ (curved)
0°	0.00×10^{0}	0.00×10^{0}	0.00×10^{0}
2°	2.24×10^{-2}	1.58×10^{-3}	6.32×10^{-3}
4°	4.16×10^{-2}	2.61×10^{-3}	1.22×10^{-2}
6°	4.32×10^{-2}	3.23×10^{-3}	1.71×10^{-2}
8°	5.65×10^{-2}	3.72×10^{-3}	2.07×10^{-2}
10°	2.50×10^{-3}	4.21×10^{-3}	2.36×10^{-2}
12°	1.92×10^{-2}	4.54×10^{-3}	2.58×10^{-2}
15°	5.65×10^{-2}	4.77×10^{-3}	2.85×10^{-2}
Max.	5.65×10^{-2}	4.77×10^{-3}	2.85×10^{-2}

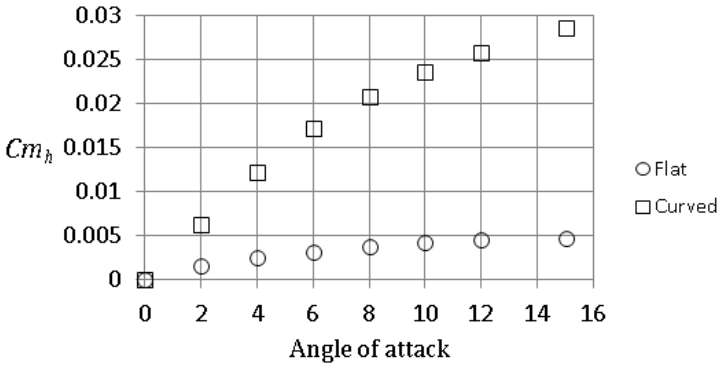

Figure 4.22: Hinge moment coefficients of the curved and the flat grid fin models

CHAPTER 5

CONCLUSION & FUTURE WORK

In this thesis study, grid fin control devices in transonic flight regime are studied by means of theoretical assessments and computational efforts. After introducing typical characteristics of grid fins, a new design methodology, which is useful for design of grid fins of missiles in transonic flight, is explained and it is applied to an example case.

Behavior of grid fins in different flow regimes is investigated. Typical characteristics within transonic flight, which are of main interest in this thesis, are observed and associated with mathematical models. The most important finding is that the choked flow within the cells of a grid fin can be analyzed by the converging nozzle analogy.

Grid fin design procedure is explained and 'unit grid fin' concept, which is developed and used in current thesis study, is introduced as a CFD model. This model significantly reduces the requirement for computational efforts.

A sample design effort is conducted for transonic flight ($M = 0.75$) in order to obtain an equivalent control characteristics with one of the widely known generic missile geometries having regular planar fins. In this study, a grid fin geometry is created and mounted to the same missile body, instead of planar fins. At the end of the design study, an alternative design that leads to the least drag force is chosen. It is seen that a more efficient design is accomplished when compared to baseline planar fin design in terms of drag and hinge moment characteristics. Hinge moment of the grid fin is found less than one tenth of minimum possible

hinge moment of the planar fin. Although drag force on the new grid fin design is calculated slightly less than drag force on baseline planar fin, this result might be unrealistic since the drag force strongly depends on frame & rod thicknesses, whose values are not verified to fulfill the structural requirements.

A simple change in the grid fin geometry is made to obtain the curved grid fin, which is desired in order to stow the fins more compactly. This geometry does not only provide a more effective packaging, but it also yields less drag force for the complete missile without changing control and stability characteristics. Drag reduction is achieved up to 4% by utilizing the curved grid fin. The drawback of using the curved grid fins is observed as relatively high magnitudes of hinge moment.

Following important conclusions are made after current thesis study:

1. Choking and all other undesired occurrences can be avoided by adjusting dimensional parameters properly.
2. Unit grid fin (UGF) concept can be utilized in order to reduce computational costs and it provides satisfactory accuracy for the low transonic range of flight conditions.
3. '×' configuration should be preferred for arrangement of grid fins on a missile body.
4. Transonic operation of missiles with grid fins is possible with a careful design.
5. Validity of UGF approach improves as the number of cells in a grid fin increases.
6. Grid fins have a potential to perform at least as efficiently as planar fins in transonic flight regime.
7. Curved grid fins can be utilized to achieve a more compact packaging and lower transonic drag force.

Following research items are addressed as future work:

1. A similar design procedure is planned to be applied for low and high supersonic regimes.

2. High angle of attack behavior of the grid fin is planned to be investigated to characterize the linear response range, which is crucial in robustness of control algorithm.

3. The sample design in current thesis study constitutes an aerodynamic database for changing parameters within certain geometric restrictions. This database is planned to be enlarged considering different geometric and structural restrictions.

4. The design procedure is planned to be applied on various missile body types possessing different static stability characteristics.

5. Roll control characteristics and their effect on the design of the grid fin should also be covered in the future.

6. Frame profile is one of the items that is not covered in current thesis. It is also important parameter in decreasing drag force as well as being a structural member. Therefore, its optimization should be addressed in the future.

7. Length of the connecting rods are also one of the parameters that is not studied in this thesis. Determination of this parameter is also planned to be studied in the future.

REFERENCES

[1] SpaceX CRS-5: Grid-fins and a barge - SpaceFlight Insider. http://www.spaceflightinsider.com/missions/commercial/spacex-crs-5-landing-barge-grid-fins/. (Visited on 05/16/2015).

[2] Wikipedia. R-77 — Wikipedia, the free encyclopedia, 2014. [Online; accessed 14-November-2014].

[3] E. L. Fleeman. *Tactical Missile Design.* American Institute of Aeronautics and Astronautics, Inc., Reston, VA, 2001.

[4] Missile aerodynamic control | electronics world. http://elektroarsenal.net/missile-aerodynamic-control.html. (Visited on 18-March-2015).

[5] Aerospaceweb.org | ask us - missile grid fins. http://www.aerospaceweb.org/question/weapons/q0261.shtml. (Visited on 22-March-2015).

[6] Wikipedia. BGM-71 TOW — Wikipedia, the free encyclopedia, 2015. [Online; accessed 25-March-2015].

[7] S. M. Belotserkovsky, L. A. Odnovol, Y. Z. Safin, A. I. Tylenev, V. P. Frolov, and V. A. Shitov. *Reshetchatye Krylya (Lattice Wings).* Mashinostroenie, Moscow (in Russian), 1985.

[8] Y. Zeng, J. Cai, M. Debiasi, and T. L. Chng. Numerical study on drag reduction for grid-fin configurations. In *47th AIAA Aerospace Sciences Meeting Including The New Horizons Forum and Aerospace Exposition*, AIAA-2009-1105, Orlando, FL, USA, January 2009.

[9] J. E. Burkhalter and H. J. Frank. Grid fin aerodynamics for missile applications in subsonic flow. *Journal of Spacecraft and Rockets*, 33(1), January-February 1996.

[10] J. E. Burkhalter, R. J. Hartfield, and T. M. Leleux. Nonlinear aerodynamic analysis of grid fin configurations. *Journal of Aircraft*, 32(3):547–554, May-June 1995.

[11] P. Theerthamalai. Aerodynamic characterization of grid fins at subsonic speeds. *Journal of Aircraft*, 44(2):694–697, March-April 2007.

[12] R. W. Kretzschmar and J. E. Burkhalter. Aerodynamic prediction methodology for grid fins. In *RTO AVT Symposium on "Missile Aerodynamics"*, pages 11–1—11–11, Sorrento, Italy, May 1998.

[13] G. M. Simpson and A. J. Sadler. Lattice controls: A comparison with conventional, planar fins. In *RTO AVT Symposium on "Missile Aerodynamics"*, pages 9–1—9–10, Sorrento, Italy, May 1998.

[14] D. Washington and M. S. Miller. Experimental investigations of grid fin aerodynamics: A synopsis of nine wind tunnel and three flight tests. In *RTO AVT Symposium on "Missile Aerodynamics"*, pages 10–1—10–14, Sorrento, Italy, May 1998.

[15] S. Munawar. Analysis of grid fins as efficient control surface in comparison to conventional planar fins. In *27th International Congress of the Aeronautical Sciences*, Nice, France, September 2010.

[16] P. Reynier, U. Reisch, J.-M. Longo, and R. Radespiel. Flow predictions around a missile with lattice wings using the actuator disc concept. *Aerospace Science and Technology*, 8(5):377 – 388, 2004.

[17] H. S. Prashanth, K. S. Ravi, and G. B. Krishnappa. Aerodynamic characteristics of G16 grid fin configuration at subsonic and supersonic speeds. *International Journal of Engineering Research and General Science*, 2:129–135, August-September 2014.

[18] J. DeSpirito, M. E. Vaughn Jr., and W. D. Washington. Numerical investigation of aerodynamics of canard-controlled missile using planar and grid tail fins, part ii: Subsonic and transonic flow. Technical report, U.S. Army Research Laboratory, March 2004.

[19] G. Abate and R. Duckerschein. Subsonic/transonic free-flight tests of a generic missile with grid fins. In *38th AIAA Aerospace Sciences Meeting and Exhibit*, AIAA-2000-0937, Reno, NV, USA, January 2000.

[20] G. Abate, G. Winchenbach, and W. Hathaway. Transonic aerodynamic and scaling issues for lattice fin projectiles tested in a ballistic range. In *19th International Symposium of Ballistics*, Interlaken, Switzerland, May 2001.

[21] J. DeSpirito and J. Sahu. Viscous CFD calculations of grid fin missile aerodynamics in the supersonic flow regime. In *39th AIAA Aerospace Sciences Meeting and Exhibit*, AIAA-2001-0257, Reno, NV, USA, January 2001.

[22] J. DeSpirito, H. L. Edge, J. Sahu, and S. P. G. Dinavahi. Computational fluid dynamics analysis of a missile with grid fins. *Journal of Spacecraft and Rockets*, 38(5):711–718, September-October 2001.

[23] J. E. Kless and M. J. Aftosmis. Analysis of grid fins for launch abort vehicle using a cartesian Euler solver. In *29th AIAA Applied Aerodynamics Conference*, AIAA-2011-3666, Honolulu, HW, USA, June 2011.

[24] P. Theerthamalai and M. Nagarathinam. Aerodynamic analysis of grid-fin configurations at supersonic speeds. *Journal of Spacecraft and Rockets*, 43(4):750–756, July-August 2006.

[25] M. C. Hughson and E. L. Blades. Transonic aerodynamic analysis of lattice grid tail fin missiles. In *24th AIAA Applied Aerodynamics Conference*, AIAA-2006-3651, San Fransisco, CA, USA, June 2006.

[26] M. Debiasi, Y. Zeng, and T. L. Chng. Swept-back grid fins for transonic drag reduction. In *28th AIAA Applied Aerodynamics Conference*, AIAA-2010-4244, Chicago, IL, USA, June 2010.

[27] Y. Zeng. Drag reduction for sweptback grid fin with blunt and sharp leading edges. *Journal of Aircraft*, 49(5):1526–1531, September-October 2012.

[28] D. Washington, P. F. Booth, and M. S. Miller. Curvature and leading edge sweep back effects on grid fin aerodynamic characteristics. In *11th AIAA Applied Aerodynamics Conference*, AIAA-93-3480-CP, Monterey, CA, USA, August 1993.

[29] Y. Li, J. Shan, J. Su, and Y. Huang. Numerical simulation on circular-arc grid fin configurations. *Applied Mechanics and Materials*, 444-445:342–346, October 2013.

[30] E. Schülein and D. Guyot. Novel high-performance grid fins for missile control at high speeds: Preliminary numerical and experimental investigations. Technical report, DLR, Institut für Aerodynamik und Strömungstechnik, May 2006.

[31] K. S. Orthner. Aerodynamic analysis of lattice grid fins in transonic flow. Master's thesis, Air Force Institute of Technology, 2004.

[32] E. Dikbaş, Özgür Uğraş Baran, and C. Sert. A 2-D theoretical and computational study for preliminary determination of grid fin geometric parameters at low transonic speeds. In *7th Ankara International Aerospace Conference*, AIAC-2013-049, Ankara, Turkey, September 2013.

[33] J. D. Anderson. *Modern Compressible Flow: With Historical Perspective*. McGraw Hill Companies, Inc., New York, NY, 2003.

[34] Fluent Inc. *FLUENT 6.3 User's Guide*, September 2006.

[35] C. Hirsch. *Numerical Computation of Internal and External Flows: Computational Methods for Inviscid and Viscous Flows*, volume 2. Wiley, 1990.

[36] D. Washington and M. S. Miller. Grid fins - a new concept for missile stability and control. In *31st AIAA Aerospace Sciences Meeting and Exhibit*, AIAA-93-0035, Reno, NV, USA, January 1993.

[37] M. H. Aksel and O. C. Eralp. *Gas Dynamics*. Prentice Hall, New York, NY, 1993.

[38] Fluent Inc. *FLUENT 14.0 Theory Guide*, November 2011.

[39] W. C. Pitts, J. N. Nielsen, and G. E. Kaattari. Lift and center of pressure of wing-body-tail-combinations at subsonic, transonic, and supersonic speeds. Technical report, National Advisory Committee for Aeronautics, January 1957.

[40] A. Dupuis. Aeroballistic range and wind tunnel tests of the basic finner reference projectile from subsonic to high supersonic velocities. Technical report, Defence R&D Canada Valcartier, October 2002.

[41] I. Shantz and R. T. Groves. Dynamic and static stability measurements of the basic finner at supersonic speeds. Technical report, U.S. Naval Ordnance Laboratory, January 1960.

[42] Z. L. Zhao, H. B. Wang, Y. Tao, and Y. J. Wang. Predictions of dynamic damping coefficients of basic finner based on CFD. *Applied Mechanics and Materials*, 380:215–218, 2013.

[43] J. DeSpirito. Lateral reaction jet flow interaction effects on a generic fin-stabilized munition in supersonic crossflows. Technical report, U.S. Army Research Laboratory, November 2013.